IEEE Access
Multidisciplinary | Rapid Review | Open Access Journal

Received February 21, 2020, accepted March 3, 2020, date of publication March 16, 2020, date of current version March 25, 2020.

Digital Object Identifier 10.1109/ACCESS.2020.2980961

Machine Learning Applied to Electrified Vehicle Battery State of Charge and State of Health Estimation: State-of-the-Art

CARLOS VIDAL, (Student Member, IEEE), PAWEL MALYSZ, (Senior Member, IEEE), PHILLIP KOLLMEYER, (Member, IEEE), AND ALI EMADI, (Fellow, IEEE)
McMaster Automotive Resource Centre (MARC), McMaster University, Hamilton, ON L8P 0A6, Canada
Corresponding author: Carlos Vidal (vidalc2@mcmaster.ca)

ABSTRACT The growing interest and recent breakthroughs in artificial intelligence and machine learning (ML) have actively contributed to an increase in research and development of new methods to estimate the states of electrified vehicle batteries. Data-driven approaches, such as ML, are becoming more popular for estimating the state of charge (SOC) and state of health (SOH) due to greater availability of battery data and improved computing power capabilities. This paper provides a survey of battery state estimation methods based on ML approaches such as feedforward neural networks (FNNs), recurrent neural networks (RNNs), support vector machines (SVM), radial basis functions (RBF), and Hamming networks. Comparisons between methods are shown in terms of data quality, inputs and outputs, test conditions, battery types, and stated accuracy to give readers a bigger picture view of the ML landscape for SOC and SOH estimation. Additionally, to provide insight into how to best approach with the comparison of different neural network structures, an FNN and long short-term memory (LSTM) RNN are trained fifty times each for 3000 epochs. The error is somewhat different for each training repetition due to the random initial values of the trainable parameters, demonstrating that it is important to train networks multiple times to achieve the best result. Furthermore, it is recommended that when performing a comparison among estimation techniques such as those presented in this review paper, the compared networks should have a similar number of learnable parameters and be trained and tested with identical data. Otherwise, it is difficult to make a general conclusion regarding the quality of a given estimation technique.

INDEX TERMS Machine learning, artificial intelligence, deep learning, battery management systems (BMS), electric vehicles, state of charge, state of health.

LIST OF SELECTED ABBREVIATIONS

BMS	Battery Management System
BOL	Beginning of Life
CC/CV	Constant-Current Constant Voltage profile
ECM	Equivalent Circuit Model
EIS	Electrochemical Impedance Spectroscopy
EOL	End of Life
FLOPS	Floating-Point Operations per Second
HPPC	Hybrid Pulse Power Characterization
KF	Kalman Filter
LFP	Lithium Iron Phosphate (cathode: LiFePO4; anode: C)
LTO	Lithium Titanate anode (cathode: Not Informed; anode: Li4Ti5O12)
MAE	Mean Absolute Error
MSE	Mean Squared Error
NCA	Lithium Nickel Cobalt Aluminum Oxide (cathode: LiNiCoAlO2; anode: C)
NMC	Lithium Nickel Cobalt Manganese Oxide (cathode: LiNiCoMnO2; anode: C)
OCV	Open-Circuit Model
RMSE	Root Mean Squared Error
SOHc	State-of-Health based on battery capacity loss
SOHr	State-of-Health based on the increase of battery resistance
SOP	State-of-Power
xEV	Electrified Vehicle

The associate editor coordinating the review of this manuscript and approving it for publication was Alberto Cano.

I. INTRODUCTION

The transportation industry faces many challenges to improve efficiency, expand performance, advance connectivity, increase autonomy, and reduce emissions. Some of the biggest automotive markets, the USA and China, have established targets to reduce CO_2 emissions by 12% and 18% respectively from 2017 to 2020 [1]. The electrified powertrain is one of the most effective technologies to enable the improvement of vehicle efficiency, but finding the best trade-off between efficiency and costs remains a great challenge [2]. As the battery remains one of the most expensive parts of the xEV [3], properly estimating the battery states are crucial to reducing overdesign costs and increasing the overall vehicle efficiency and performance. As a result, significant design effort is placed on the battery management system (BMS) software design to perform a state of charge (SOC) and state of health (SOH) estimation accurately.

Most of the practical SOH methods for capacity estimation are based on amp-hour (Ah) counting between precise reference SOC points. SOH methods for resistance estimation are more varied and range from simple averaging of delta voltage divided by delta current to recursive algorithms such as recursive least squares or advanced Kalman filter (KF) algorithms [6]. In the case of SOC estimation, one of the simplest methods is based on open-circuit voltage (OCV) and coulomb counting. However, more robust and sophisticated methods are preferred to handle sensor errors and uncertain model knowledge [4], [5]. Many approaches employ an equivalent circuit model (ECM) combined with KF variants for SOC estimation [6], [7]. To make these approaches work well, significant battery testing is needed to model and parameterize the algorithms. For a comprehensive review of the different approaches to the estimation of SOC, SOH, SOP, and other battery states, beyond the machine learning approaches, which are the focus of this paper, readers are referred to [4], [6], [7].

Machine learning data-driven approaches to battery state estimation have been driven by recent advances in artificial intelligence (AI) [8] in fields such as computer vision and autonomous vehicles. The Venn diagram in Fig. 1 shows how the field of AI is subdivided, including Machine Learning and its subsequent divisions of representation learning and deep learning [9]. Fig. 1 also shows how the scope of this survey paper, the state of the art of machine learning SOC and SOH estimation methods for electrified vehicles (xEVs), is bounded within the AI field while permeating all subfields of machine learning. Fig. 2 shows a structured summary of the SOC and SOH estimation methods considered and analyzed in this paper. For a comprehensive explanation of ML itself and its basic math, interested readers are referred to [9], [10].

As battery technology grows and matures, a significant amount of data is being collected and analyzed in a partially or fully automated fashion [11] to improve battery design and usage. This plethora of data has made it possible to improve

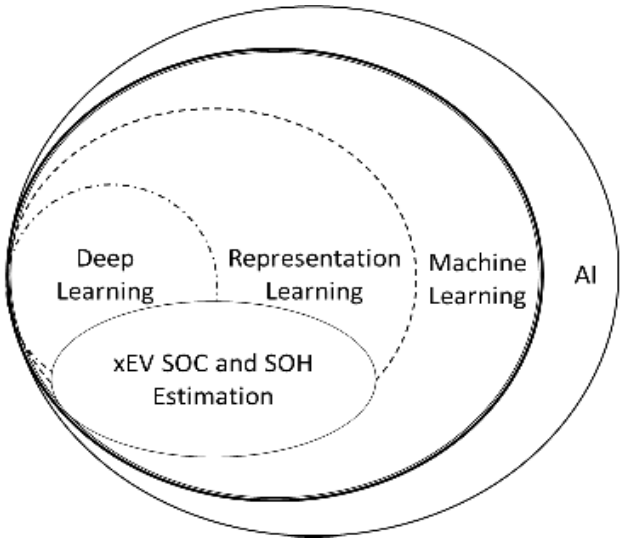

FIGURE 1. Venn diagram [9] showing the relation of xEV SOC and SOH Estimation to the field of artificial intelligence and machine learning.

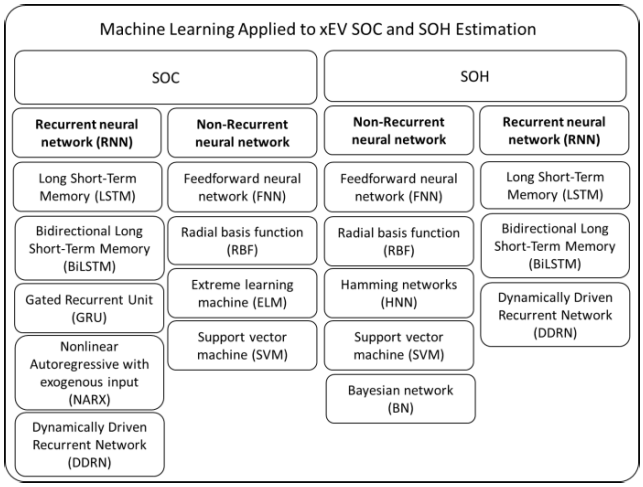

FIGURE 2. Structured summary of the ML methods considered and analyzed in this paper.

BMS performance [12] via big data, the internet of things (IoT), cloud computing, and the ML methods investigated here. In the case of SOC and SOH estimation based on ML methods, the main computational load demanded by these approaches happens during its off-line training phase [13], making it feasible for implementation on typical BMS hardware.

The remainder of the paper is structured as follows: Section II reviews ML methods for SOC estimation, Section III focuses on SOH estimation, and Section IV gives concluding remarks.

II. BATTERY STATE OF CHARGE ESTIMATION

This section presents relevant published work regarding the estimation of battery SOC using machine learning methods. The battery SOC is the equivalent of a fuel gauge used in traditional gasoline vehicles. Although, unlike the fuel gauge,

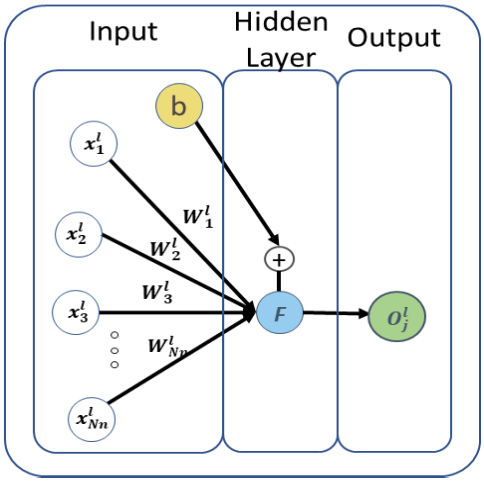

FIGURE 3. One hidden layer perceptron.

to determine the percentage of useful energy left inside the battery, it is necessary to perform an indirect measurement of the SOC via estimation. This is done by a great variety of methods and techniques which use measurable signals such as the battery terminal voltage, current, and temperature [4]. This is not an easy task due to the nonlinear nature of the battery. An accurate estimation of the SOC is crucial to improve vehicle performance, safety, passenger comfort, and to minimize costs associated with over design or oversizing of the pack.

In the remainder of this section, different ML SOC estimation methods which have been utilized in the most recent literature will be presented as follows:

A. Feedforward neural network (FNN)
B. Radial basis function (RBF) neural network
C. Extreme learning machine (ELM)
D. Support vector machine (SVM)
E. Recurrent neural network (RNN)

A. FEEDFORWARD ARTIFICIAL NEURAL NETWOR

An FNN implements non-linear mappings with an arbitrary number of inputs and outputs. It is one of the simplest neural networks (NNs) to apply. Fig. 3 shows a simple one hidden layer perceptron FNN structure with multiple inputs and a single output. Besides the structure of the FNN, a nonlinear activation function F must also be selected a priori. A common choice is the hyperbolic tangent function, equation (1) below, which limits the output to values between 1 and -1. Alternatively, a rectified linear unit (RELU), as shown in (2), can be chosen and consists of a function that sets all negative input values to zero.

$$F(x) = \frac{2}{1 + e^{-2x}} - 1 \tag{1}$$

$$F(x) = max\ (0, x) \tag{2}$$

The training process aims to find the values of the learnable parameters, the weights W_N^l and bias b for the one layer perceptron, to minimize a sum of the squared error loss function. Training is frequently performed using a backpropagation algorithm [10], which computes the partial derivative of the estimated cost (error) relative to the weight and bias values and then updates their values to reduce the computed cost iteratively. The number of training iterations performed over the entire dataset is referred to as the number of epochs and is typically used to derive a stop condition for the training process. Depending on the training algorithm, other conditions can also be used to end the process, such as stopping based on the rate of improvement of the error.

1) FNN COMBINED WITH FILTERS AND OTHER MODELS

A hybrid approach, which has combined the use of an ECM and FNN, was presented by [14], which, instead of using a lookup table (LUT) to correlate the battery SOC to the battery OCV, an FNN model was trained to make this correlation. The FNN structure was formed by one input, the OCV, a hidden layer with m neurons, and the SOC as its output. With the FNN model capable of correlating the SOC based on the OCV input, an ECM was developed to estimate the OCV based on the battery terminal voltage. In [15], and FNN was built to estimate the SOC of an LFP battery and an Unscented Kalman filter was then used to improve the SOC estimation accuracy. The FNN presented in [15] is a supervised ML algorithm, which is characterized by the use of a known reference or target employed to calculate the ML output estimation error. To train the FNN in this work, a set of battery data was acquired using the automotive homologation driving cycles US06, FUDS and the dynamic stress test (DST) specified by the U.S. Advanced Battery Consortium (USABC). Although in this case, the amount of data seems to be a very narrow representation of the application domain, which can explain the relatively low accuracy when tested in the US06 dataset, as shown in Table 2, despite the use of UKF to improve the accuracy.

2) FNN DIRECTLY USED FOR SOC ESTIMATION

A work using an FNN, but without the use of a Kalman filter, was presented in [11] for a 12V hybrid energy storage system. This system was composed of a 12V LFP battery and a 12V lead-acid battery to power a belt starter generator system where the electric machine functioned as either a motor or generator according to the control strategy, which kept the Li-ion battery cycling within a partial SOC window. An FNN was developed to simultaneously estimate the SOC of both batteries using the same neural network structure. However, a benchmark comparison with two separate single-output NN models that estimate SOC of each cell type was not performed. Such comparison needs to be further investigated to clarify the benefits of the shared NN dual SOC estimation output approach.

Because different sources influence the Li-ion batteries' characteristics, e.g., SOC, SOH, current, and temperature [16], the authors in [17], have considered the use of the battery polarization states as inputs for an FNN model trained to estimate battery SOC. The polarization states can have a

significant influence on the battery terminal voltage [18] and can be calculated from the battery current using equation (3), where S_k is the polarization state at sample point k, Δt_i the sampling interval, N the number of parts within the interval Δt_i, $i_{L,k}$ the battery current, and τ the time constant that can have any integer value from 0 to 1000.

$$S_k = exp\left(-\frac{1}{\tau}\sum_{i=k}^{N}\Delta t_i\right)S_0 + \left(1 - exp\left(-\frac{1}{\tau}\sum_{i=k}^{N}\Delta t_i\right)\right)i_{L,k} \quad (3)$$

The authors have investigated the use of different values of τ and multiple polarization state inputs. In the end, four values of $\tau = [2, 6, 32, 155]$, were chosen for the four polarization states, together with the battery current, voltage, and temperature as inputs to the FNN. The FNN was trained and tested with measured data from an NCA cell for ten standard drive cycles including the EUDC, HL07, HWFET, LA92, NEDC, MANHATTAN, NYCC, REP05, SC03, and UNIF01, each performed at ambient temperatures of −10°C, 0°C, 10°C, and 25°C. From the entire dataset, 80% was used to train and the remaining 20% for validation and testing. The model was further tested in the lab on a Hardware In the Loop (HIL) system. This paper is an example of a thorough study that includes a complex dataset and a good division of training and testing data.

In [13], the authors have shown that the FNN is capable of estimating battery SOC at different temperatures, including temperatures as low as −20°C. Although FNNs are not capable of storing and using past information from a time series, it is possible to encode this information partially by creating new input features based on the moving average of the battery terminal voltage and current. This technique seems to work well as the results obtained are equivalent to those obtained by RNNs, which will be discussed in detail in the next section. Here the authors have systematically evaluated different numbers of neurons, the number of hidden layers, and the average based on two different sample windows (100 and 400 timesteps). The FNN architecture used in this work is depicted in Fig. 4, where the inputs are the battery terminal voltage $V(k)$, battery temperature $T(k)$, averaged terminal voltage V_{avg}, averaged current I_{avg}, and the output is SOC at timestep k. The best result at 25°C was obtained when a rolling window of 400 timesteps was used. As expected, the errors are much higher at −20°C due to the low temperature effects on the li-ion batteries [16]. It was conjectured that it might be improved if a larger dataset was used and a more complex FNN was built to capture all the complexity presented at low temperatures. Another contribution from the authors shows that using so-called augmented datasets can improve the robustness and accuracy of the model by up to 41%.

In [19] the authors have used the internal resistance data, obtained from a tester in the lab, along with the voltage, current and battery temperature, to train and test an FNN to estimate SOC, although the use of the internal resistance would

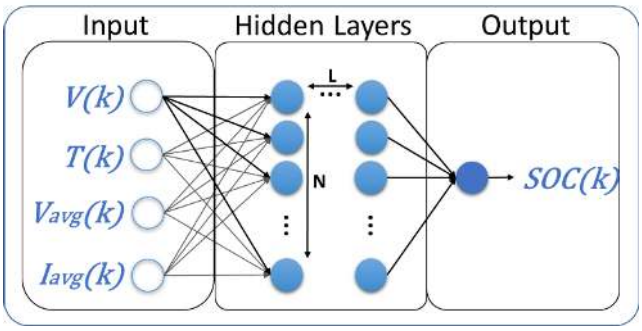

FIGURE 4. FNN structure used to estimate battery SOC [13], where the battery terminal voltage V(k), battery temperature T(k), averaged terminal voltage V_{avg}(k), and averaged current $I_{avg}(k)$, are used as input, and the output is SOC at timestep k.

be a valuable input feature, not only for SOC but also for SOH estimation, its direct measurement in a vehicle would be difficult due to practical reasons. Alternatively, using a model to estimate the battery's internal resistance is possible and can be implemented onboard to provide real-time input information [20].

The authors in [21] introduced a process to systematically alter the FNN structure using offline optimization algorithms to find the optimal FNN structure. The work has focused on the backtracking search algorithm, an optimization algorithm, which according to the authors is easier to implement, faster, and more robust when compared to other algorithms, such as a genetic algorithm (GA), particle swarm optimization (PSO), and artificial bee colony. The backtracking search algorithm (BSA) was set to optimize the number of neurons in the hidden layer and the learning rate value. The procedure of this work was divided into four stages. In the first stage, the data was collected from an 18650 NMC lithium battery cell with 2 Ah capacity using DST and FUDS cycles, then filtered and normalized. On stage two, the SOC is estimated using a chosen primary structure to calculate the initial cost (root mean squared error) to be used in the next stage. On stage three, the backtracking search algorithm is applied to find the number of neurons in the hidden layer, and the learning rate in which makes the SOC estimation error the lowest. This procedure was applied with other learning algorithms instead of FNN for comparison, and the battery data was acquired at three different temperatures; 0°C, 25°C, and 45°C. An individual FNN model structure was established using BSA for each dataset at each temperature, and it was noted that at 0°C, the errors obtained in each method are about double the error when comparing the results at 25°C. Ideally, one FNN model should be able to handle different temperatures if appropriately trained, as previously shown in [13].

There is a great potential of using optimization algorithms to help determine the FNN structure and therefore reducing the necessity of previous engineering experience to set the "correct" FNN training parameters. Although many other parameters besides the number of neurons and learning rates should be considered, e.g., the number of hidden layers,

the initial weights distribution values, it will also increase complexity and the offline computational burden for the search of the optimal structures.

Another unique approach was presented by the authors in [22], where they have trained a model composed of three parallel FNNs, each individually trained with distinct training data from three operation modes, idling, charging, and discharging. Despite the low accuracy and limited data used to train and test the FNN (US06 for validation and testing and pulsed profile for training), the authors have considered the impact of random initial NN weights by performing training 50 times and using the average error as the final result of the method. The authors show that the initial values, which are generally randomly selected when training an NN, can lead to different local minima. Despite the importance of initial parameters on training, their effect on the result is explicitly considered in only a few of the publications presented in this survey.

B. RADIAL BASIS FUNCTION NEURAL NETWORK

A radial basis function neural network is a class of FNN that contains only an input layer, one hidden layer, and an output layer implementing linear summation. Rather than use nonlinear monotonic single-valued activation functions, the hidden layer neurons in an RBF compute a Euclidean distance, multiply it by a (standard deviation related) scaling factor, and map it through a Gaussian function. This is also referred to as a radiated Gaussian kernel function (4).

$$\varphi_i(\boldsymbol{x}) = G\left(||\boldsymbol{x} - \boldsymbol{w}_i||\right) = exp\left(-\frac{||\boldsymbol{x} - \boldsymbol{w}_i||^2}{\sigma_i^2}\right) \tag{4}$$

An example RBF neural network is shown in Fig. 5. Rather than determining weight gains in the training process, centroid vectors are fitted in the RBF neural network training stage. RBF neural networks are also typically characterized as having very fast training/learning and being good at interpolation [46].

A radial basis function neural network with an extended Kalman filter (EKF) was used in [23], [24] for online estimation of the SOC of a Li-ion battery cell and a lead-acid battery. In this work, a battery model was first created using the RBF structure to find the state-space equations for the EKF. The state variables extracted from the battery model were the SOC and terminal voltage from the previous time step. The temperature used in this work was only the ambient room temperature. A similar use of the RBF was presented in [25] and [26], although using extended H_∞ and unscented Kalman filter (UKF), respectively.

In [27], the authors used the RBF to learn the dynamics of a lithium polymer battery cell trained offline with experimental battery data to estimate the SOC. The trained RBF was then used to establish the upper bounds of the system uncertainties adaptively, and to determine a parameter necessary for the determination of the appropriate switching gain which is essential for robustness. Through the Lyapunov stability theory, the sliding variables converge theoretically to the sliding surface and remain there for a finite time until the error asymptotically converges to zero [28]. The upper bound is adaptively updated by an RBF, using the structure in Fig. 5, providing robust traceability and limiting the chattering magnitudes in the SOC estimation. In Fig. 5 $\hat{x}$ is the estimated state vector, φ represents the Gaussian function in each of the 9 neurons of the RBF structure and $\hat{\bar{\psi}}$ is the updated upper bound of the system uncertainty.

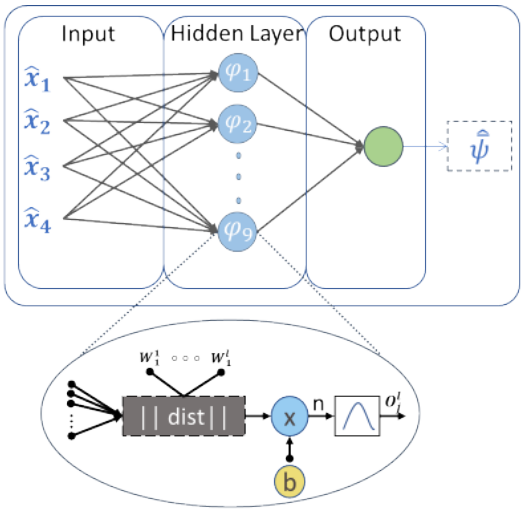

FIGURE 5. Example radial basis function neural network structure.

In [29], a multi-cell Li-ion battery pack SOC estimation framework was presented, and an RBF was used to quantify the uncertainties necessary to build a response surface model of model bias. In this work, the model bias δ is the stochastic difference between the estimated and measured li-ion cell terminal voltage. This is motivated due to the intrinsic differences between each cell in the battery pack, which makes it challenging to track their dynamics accurately. After quantifying the parameter uncertainties using the RBF, it was possible to apply the average pack model to each cell and have a better estimation of the terminal voltage. Then an adaptive extended Kalman filter (AEKF) was applied to perform an online SOC estimation of the entire pack.

C. EXTREME LEARNING MACHINE

The extreme learning machine (ELM) structure is very similar to an FNN, but the main difference consists of its training algorithm, which instead of using backpropagation, the ELM uses the Moore-Penrose generalized inverse or pseudoinverse matrix [30]. In [31], the authors used an ELM to model a Li-ion battery from experimental data; then, the SOC estimation was approximated using a KF. The ELM method was compared with an RBF showing lower computational load and better SOC estimation error. Besides, four different KF algorithms were compared: EKF, AEKF, UKF, and adaptive unscented Kalman filter (AUKF). As shown in Fig. 6, the ELM was used to estimate the battery terminal

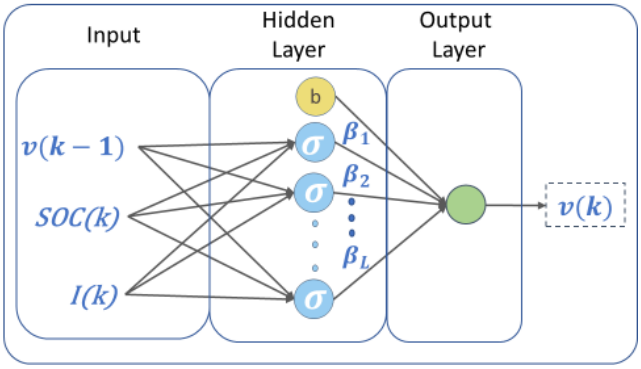

FIGURE 6. ELM network structure to model the battery terminal voltage [31].

voltage $V_{(k)}$, based on the battery current $I_{(k)}$, $SOC_{(k)}$ using SOC-OCV relation, and $V_{(k-1)}$, which is the terminal voltage from the previous sample step.

The ambient temperature used in this work was 25°C, and the number of neurons used was 10 and 15 for both ELM and RBF, respectively. The ELM were up to 50% faster when compared to the RBF estimation time and have provided lower estimation error. Moreover, the use of the AUKF for SOC estimation improved its accuracy and reduced the computational load, even when comparing with other variations of KFs.

In [32] the authors have used the gravitational search algorithm (GSA) to find the optimal number of neurons in an ELM with one hidden layer for two different drive cycles, US06 and Beijing dynamic stress test (BJDST) at two different temperatures (25°C and 45C°); however, they have used what seems to be a limited dataset to validate the generalization capability of the ELM model for xEV applications. Instead of training and validating the model using different drive cycles, only a portion of the same drive cycle data was used to train and validate the model, 70% for training and 30% for validation. Their use of optimization algorithms seems to be a promising path to automate the process of ML structure selection.

D. SUPPORT VECTOR MACHINE

The SVM was initially created to solve logistic/classification problems. In most cases, battery SOC estimation requires a regression learning method, which sequentially minimizes the error function. The generalized regression variation of SVM, known as support vector regression (SVR), can be employed. This technique aims to solve a regression problem for data that is not linearly separable. This approach shares some similarities to the RBF methods previously described. However, a crucial distinction is that SVR aims to employ simplified optimization routines such as quadratic programming with linear constraints to fit the SVR parameters. Moreover, the concept of an error tolerance margin is used such that no cost function penalty is applied to the fitting error if it is within some defined error band; this, in principle, should stabilize the estimation.

In [33], an SVM was applied to estimate the SOC of a 60Ah LFP. The concept of a kernel was used to compute the support vectors. The most popular kernel is RBF, similar to equation (4); however, polynomial kernels are also possible [34]. The fitted support vector lies in a high dimensional hyperspace; in particular, 903 support vectors were found to be optimal in this case. The battery data in this work was obtained from a dynamic profile where the terminal voltage, current, and ambient temperature were employed. Similar work based on data from a 100Ah cell was performed by the same research group in [34].

E. RECURRENT NEURAL NETWORK

In this section, different types of RNNs are introduced and the most critical points found in recent publications are discussed. Various RNN machine learning methods that are strong candidates for SOC and SOH estimation are presented.

1) INTRODUCTION TO RNNs

The recurrent neural network is a type of neural network that uses past information in a closed-loop manner. A neural network can be made recurrent by simply passing the network output, or an intermediate state, as an input. For example, SOC of k-1 could be an input to the network at time step k. This type of ML is appropriate when short-term sequence dependencies are required but may not work as well for the long-term dependencies seen in a battery. For this type of RNN, challenges in the training process exist such that during backpropagation, the error can ''vanish'' or ''explode'' [35]. Some variations of the RNN were created to solve this limitation, such as the LSTM (shown in Fig. 7), the bidirectional LSTM (BiLSTM), and the gated recurrent unit (GRU). These are artificial neural networks structured with gates, which bridge past time data dependencies to the currently available data [36], [37]. The capacity to ''recall'' past information, makes this method especially useful to solve problems that require long sequential data or time series, e.g. speech recognition, and battery state of charge [38].

The LSTM can store and transfer information from previous and current states to be used in the future using a memory cell c_k shown in Fig. 7. The forget gate f_k is responsible to select how much of the previous information in c_{k-1} should pass ahead to the next time. The input gate i_k is responsible to regulate how much of the past information should be passed to the memory cell. The output gate o_k is responsible to control how much of the information computed in the memory cell will be included in the output h_k.

The BiLSTM, a bidirectional version of the LSTM, is a composition of a forward and backward ''unidirectional'' LSTM layer, where the forward part is fed with temporal input data Ψ starting from the earliest time-step $k - n$ to the current time-step k, $[\Psi_{k-n} \rightarrow \Psi_k]$, and the backward part it is fed in the reverse order, $[\Psi_k \rightarrow \Psi_{k-n}]$ where n is the total number of temporal steps, and y the output of the BiLSTM as shown in Fig. 8. The forward LSTMs are fed simultaneously, and the learnable parameters of each

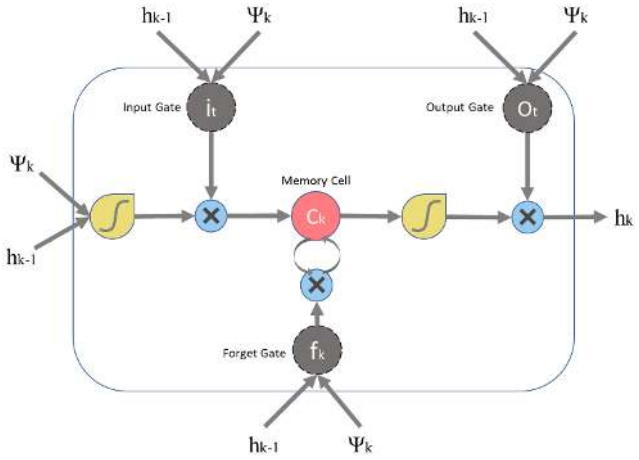

FIGURE 7. LSTM layer [37]. Ψ_k and h_{k-1} are the input data layer at the current time-step k and hidden layer at the previous time step k − 1, respectively. i_k, o_k, f_k, and C_k are the input, output, and forget gates, as well as the memory cell, respectively.

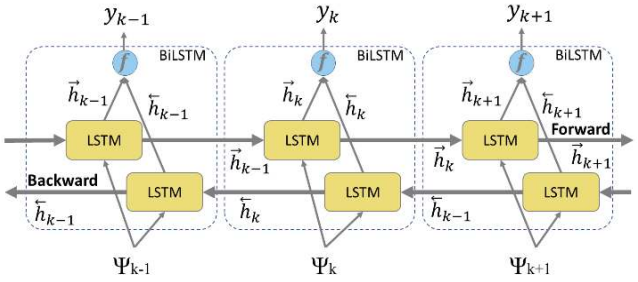

FIGURE 8. BiLSTM layer. From the forward LSTM part Ψk and $\vec{h}_{k-1}$ are respectively the input data at current time-step k and hidden layer at the previous time step k − 1, wherefrom the backward LSTM the inputs are Ψk, and $\overleftarrow{h}_{k-1}$. The BiLSTM output, y_k, are given by the combination of both forward and backward LSTMs, $\vec{h}_k$ and $\overleftarrow{h}_k$, through chosen function f.

are updated independently, but the outputs of forward, $\vec{h}_k$, and backward, $\overleftarrow{h}_k$, are combined with the function f, which can be either the concatenation, summation, multiplication or average function. The method captures temporal or contextual dependencies from both temporal ends of the data, i.e., commonly used in text translation where the end words or phrases in the text have a significant impact on the overall context and, therefore, on the correct translation. The more samples of the sequential data one can provide to the model with the BiLSTM before outputting the estimation, the better performance can be achieved, which is a limiting factor to be considered.

Another RNN approach also capable of dealing with long-term dependencies is the GRU, which employs the use of gates to learn, memorize, and decide which information from the past and the present will be used to generate its output. In contrast to the LSTM, the GRU uses a single gate unit to simultaneously control the forgetting amount and the decision to update the state unit [9]. The GRU has considerably more straightforward gate mechanisms than the LSTM and can achieve similar performance [39]. The remainder of this section is divided into two parts; 1-Gated RNNs applied to SOC estimation; 2-Other RNNs applied to SOC estimation.

2) GATED RNNs APPLIED TO SOC ESTIMATION

In [38], the authors applied an LSTM to estimate the SOC by using only direct measured battery signals, such as terminal voltage, load current, and ambient temperature, without requiring it to be coupled with other methods and estimation filters. A considerable outcome presented by this work was the capability to estimate the SOC under different temperatures. This is an advantage compared to methods that require the use of a LUT, from which it is necessary to build one LUT for each different temperature [23]. Although, it is essential to remark that this is only possible if the dataset chosen to train the LSTM includes the necessary information to encode the temperature variation within its parameters, which may lead to a large dataset. The authors used a Panasonic 18650PF Li-ion battery cell dataset acquired at multiple ambient temperatures, ranging from 0°C to 25°C; this dataset is available to download from [40].

A more recent work presented in [41], introduced a stacked BiLSTM model and compared its results with three previous publications [13], [38], [42] as the same dataset was used [40] in all four cases. The BiLSTM showed better accuracy than the other methods when the comparison was done at different temperatures, 0°C, 10°C, and 25°C. Each model in [41] was trained five times, and the average result was used as the final number for comparison, although it is not clear if the other authors in [13], [38], [42] have used training repetition, hence there is difficulty in cross-comparison among publications even though the same dataset was used. The final structure found to be optimal by the authors in [41] was composed of two stacked BiLSTMs each with 64 hidden neurons, which is equivalent to four unidirectional LSTM stacked layers and over 130,000 learnable parameters, the sum of all the weights and biases in the structure. A previous publication [43] has also used the option to increase the depth and the accuracy of the NN by stacking three LSTMs together. The stacking of LSTMs may lead to some constraints, though, such as making the network harder to train, increasing the possibility of overfitting, and increasing the number of parameters.

As a rule of thumb, the higher the number of parameters, the higher the computational cost required to run the model. This can be confirmed by addressing different aspects of the computational cost, which was investigated in regards to memory occupation in [44] as well as computational time or floating-point operations per second (FLOPS) in [43] and [45]. Another common way to compare two algorithms in terms of efficiency is using the big O notation, also known as asymptotic notation, which classifies the algorithm based on its behaviour as the number of variables and input data increases towards infinity. Big O notation was investigated and considered as a point of model comparison in [13].

Finding the right balance between model complexity and accuracy is one of the many challenges addressed and

discussed within most of the publications included in this survey. As an example, the performance similarity of the GRU and LSTM for solving speech recognition problems [39] suggests that performance similarities would also result in SOC estimation despite the obvious application differences. This assumption was initially confirmed in [42] where a GRU had been applied to perform SOC estimation using the same dataset [40] already used by the LSTM in [38]. In [46], a GRU was applied to estimate the SOC of an NMC and LFP at seven different temperatures, ranging from 0°C to 50°C. Only the FUDS, DST, and CC drive cycles were used to generate the dataset.

A combination of vector autoregressive moving average (VARMA) and an LSTM was introduced in [47] to forecast li-ion battery voltage and SOC of an electric motorcycle where a different combination of inputs, including motor speed, input power and torque, and battery voltage, current, and temperatur were evaluated. The authors have tested the model at 0°C and 25°C using only CVS-40, a South Korean driving cycle, and the data used to train the model were obtained directly from driving the motorcycle. No information about the battery, besides it being Li-ion, or the structure of the LSTM was provided, and it was not clear if the use of the VARMA in combination with the LSTM is essential when a larger dataset is available. The exploration of other features, besides the ones directly obtained from the battery, is an interesting path to pursue, for example, integrating weather forecast and/or vehicle destination.

In [48], the authors have introduced a novel way to reduce training time and further improve SOC estimation by using an LSTM with *Transfer learning,* and in [49] the authors explored the accuracy impact of using different types of loss function optimizers during model training, e.g. Adam, NAdam, Adadelta, AdaGrad, RMSProp, and AdaMax. Transfer learning and the use of appropriate optimizers are anticipated to be promising research paths that should be explored and combined with other methods.

3) OTHER RNNs APPLIED TO SOC ESTIMATION

Some publications focus on recurrent networks that do not use the gated approaches introduced in the prior section. In [50], the authors developed a dynamically driven recurrent network (DDRN) based on a nonlinear autoregressive with exogenous input (NARX) neural network architecture. The DDRN is used to estimate the SOC and SOH of two Li-ion chemistry batteries, LFP and LTO. What makes this supervised ML different from an FNN is the use of a recurrent input captured from the output of a previous state, e.g. SOC at instant k-1. This gives the DDRN an associative memory feature, despite being limited compared to the gated RNN previously discussed, this approach reduces the amount of data necessary to train the model.

The authors also showed that for SOC estimation of the LFP battery, the training time was reduced by 1000 fold compared to a ''non-recurrent'' neural network. The input dataset, containing the voltage V_k, current I_k, ambient temperature T_k, and SOC_{k-1} from the previous timestep were used to train and test the DDRN, and the data was obtained experimentally for the two batteries. The inputs and output organization on the DDRN for SOC estimation is shown in Fig. 9. The DDRN was tested at temperatures of 0°C, 10°C, 25°C, and 40°C. Even though the cycling profiles used to obtain the battery data were dynamic, they resulted in a monotonic SOC output profile because there were no regenerative braking charging pulses during the cycle. This type of profile may not be a good representation of the xEV application domain. Therefore, the effectiveness of this approach needs to be further investigated

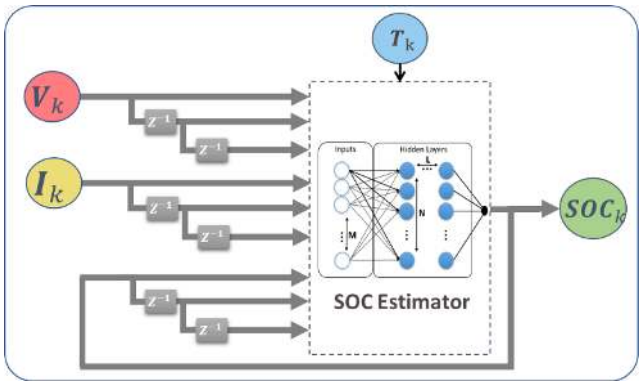

FIGURE 9. SOC estimator using DDRN, where the terminal voltage V_k, load current I_k and ambient temperature T_k are the inputs obtained by sensors and the recurrent inputs were $V_{(k-1)}$, $V_{(k-2)}$, $I_{(k-1)}$, $I_{(k-2)}$, $SOC_{(k-1)}$, and $SOC_{(k-2)}$ are the inputs from time steps $k-1$ and $k-2$.

In [45], another NARX-based neural network was presented to estimate the battery SOC. A process to systematically alter the NN structure using an offline optimization algorithm, known as lighting search algorithm (LSA), was used to find the optimal combination of the number of neurons, input delay, and feedback delay to improve the accuracy of the model. The model was trained and tested using the dataset acquired at 0°C, 10°C and, 45°C from an NMC battery cell on two drive cycles, FUDS and US06. The work also showed a comparison with other SOC estimation methods also optimized by the LSA, but the NARX was shown to provide better accuracy. Although the use of optimization algorithms like LSA and BSA can help automate and alleviate the process of searching and building the optimal NN structure, it is essential to understand that a significant number of other tuning parameters, e.g. minibatch size, loss function optimizer, and the random initialization of weights and biases can have substantial impact on the results and are often neglected.

F. EXAMPLE METHODOLOGY AND GUIDELINES FOR COMPARING SOC ESTIMATION ALGORITHMS

To provide a fair comparison of SOC or SOH estimation methods, such as those referenced in this review paper, it is necessary to evaluate each algorithm with similar data, a similar number of trainable parameters, and a consistent training and testing methodology. When comparing methods, the following three guidelines are therefore recommended:

1- *Use the same training, validation, and testing datasets*
2- *Match the number of learnable parameters between models*
3- *Train the model several times*

Regarding the first guideline, Table 3 provides references to high quality publicly available datasets that can be downloaded and used to build ML models for SOC and SOH estimation, allowing different authors, for example, to compare their results to others using the same datasets. The second guideline, to use the same number of learnable parameters, is to ensure compared models have similar computational cost and memory usage [9]. The third recommendation, to train the model several times, is necessary due to the degree of randomness embedded in the training process of ML algorithms, which can lead to several local minima. The number of repetitive training needed is highly dependent on the complexity of the model, i.e., the more parameters, hidden layers and connections, the higher the chance it can find a local minimum.

To further contribute and to support the above guidelines, an FNN and LSTM were each trained 50 times using six of the nine drive cycles from the dataset [40] and tested using the remaining three drive cycles and the constant current (CC) charge profiles, e.g. UDDS-CC-LA92-CC-NNcycle. The training and testing data used includes each drive cycle at four ambient temperatures (−10°C, 0°C, 10°C, and 25°C), forming a larger dataset composed of 24 training and 12 testing drive cycles. This resulted in 2/3 of the data being used for training and 1/3 for testing, which is similar to ratios of training to testing data, which are often recommended.

The structure of the FNN is similar to the one used in [13] and has two hidden layers, with 55 neurons in each. The input vector Ψ is composed of the battery terminal voltage, current, battery temperature, average voltage, and average current, Ψ = {V, I, T, V_avg, I_avg}, as shown in Fig. 10a. The RELU activation function was chosen for the FNN structure, and the voltage and current are averaged over the previous 500 time steps. The LSTM structure, shown in Fig. 10b, is similar to the one used in [49] and has 27 hidden units and an input vector composed by voltage, current and temperature, Ψ = {V, I, T}. The input vector for both the FNN and LSTM was rescaled to have values between 0 and 1 before being used to train the models. The total number of parameters for the FNN is 3466, and the LSTM is 3376.

The FNN and LSTM were each trained fifty times for 3000 epochs, using the hyperparameters in Table 1. Because different initial parameter values were used each time the training was performed, a different result is achieved each time. To demonstrate this, the mean average SOC estimation error over all the testing data (three drive cycles and two charges at four different temperatures) was calculated, and a histogram of the results is shown in Fig 11. The error is shown to vary from 1.2 to 1.55% for the LSTM and from 1.5 to 3.5% for the FNN. Therefore, it is recommended to train multiple

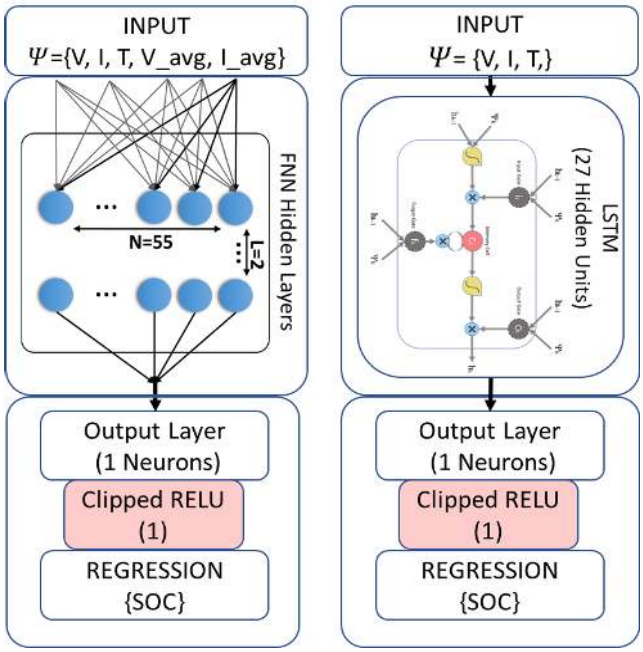

FIGURE 10. (a) FNN SOC estimator structure comprised of input vector Ψ, 55 hidden units per hidden layer, two hidden layers, and 3466 learnable parameters. (b) LSTM SOC estimator structure comprised of input vector Ψ, 27 hidden units, and 3346 learnable parameters.

TABLE 1. Training hyperparameters.

Number of epochs	3000
Initial learning rate	0.01
Learning rate drop period	2500
Learning rate drop factor	50%
Loss function optimizer	ADAM
Minibatches	89
Software platform	Matlab 2019b

times when comparing different SOC estimation structures; otherwise, it may be incorrectly concluded that one is superior to another.

G. COMPARISON OF SOC METHODS

The SOC estimation error for some of the methods presented in this section is summarized in Table 2, along with the data profiles used to train and test the methods, the network inputs and outputs, a qualitative ranking of the dataset quality, the battery type(s) used, and the temperatures investigated. Most of the studies utilize similar inputs (voltage, current, and temperature), while a few utilize averaged values or other calculated values. About half of the studies use automotive type drive cycles and/or varying temperatures, with the remainder using constant or pulsed current cycles and/or fixed temperature. The studies with simpler data sets, such as fixed temperature and constant current, are given a dataset quality rating of * and the more sophisticated datasets are ranked as high as ∗ ∗ ∗ ∗ ∗. In general, the higher the data

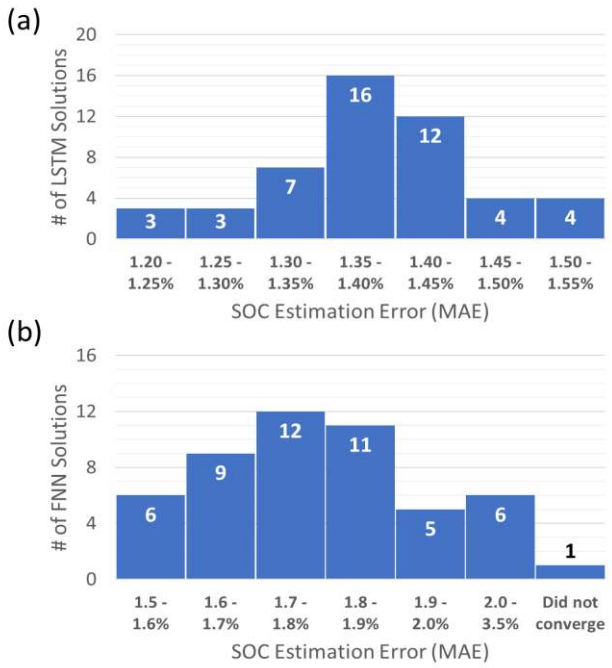

FIGURE 11. MAE histogram for 50 training iterations of SOC estimation algorithms; (a) LSTM (b) FNN.

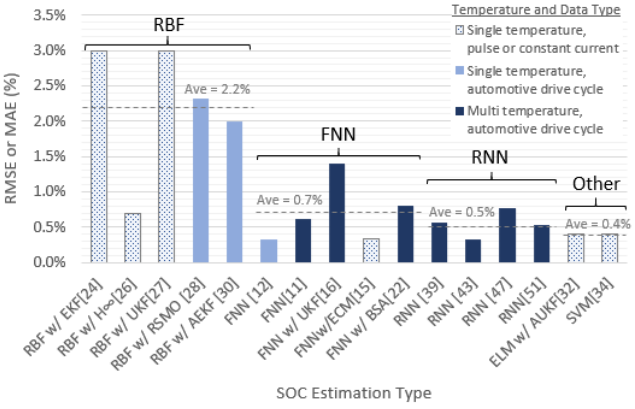

FIGURE 12. SOC estimation error, classified by method and data types.

quality, the more the stated accuracy for the method can be trusted.

Because it is difficult to come to any conclusions about the various methods by just observing the table, the accuracy of the methods is plotted in Fig. 12. The RBFs are shown to have the highest error, an average of 2.2%, with the FNNs, RNNs, and other methods having an average error of 0.7%, 0.5%, and 0.4%, respectively. The FNNs and RNNs also have more challenging multitemperature datasets with automotive drive cycles, showing that they are the most promising methods and that the other methods (ELM w/ AUKF and SVM) should be investigated with more challenging cycles to determine their potential. While these results do show some interesting trends, it is important to consider that many factors, as discussed in the prior section, affect the results for each method.

III. BATTERY STATE OF HEALTH ESTIMATION

Battery SOH is a measurement of battery deterioration in comparison to a new battery. This information is valuable for the vehicle energy management system to adjust its controls to keep the vehicle performance and safety within the desired boundaries. There are several ways to estimate and quantify the SOH of an xEV battery; many of the recent studies have considered either the loss of capacity (SOHc) or increase of internal resistance (SOHr). The conventional machine learning methods presented in this section for SOH estimation are grouped as the following types.

A. Feedforward neural network (FNN)
B. Recurrent neural network (RNN)
C. Radial basis function (RBF) neural network
D. Hamming networks (HNN)
E. Support vector machine (SVM)
F. Bayesian network (BN)

A. FEEDFORWARD NEURAL NETWORK

As previously introduced in sections I and II, an FNN performs non-linear mappings with an arbitrary number of inputs and outputs. For a more detailed explanation about the methods and its basic math, interested readers are referred to [9], [10].

For SOHc estimation, the battery capacity fading metric is typically represented by

$$SOH = \frac{C_t}{C_0} \times 100(\%) \tag{5}$$

where C_t is the capacity estimate at time t and C_o is the new battery's nominal capacity. Battery capacity is typically measured via a particular test that spans the entire SOC range using high accuracy current measurements. However, this is rarely achieved in real-world usage of an xEV, so online estimation algorithms need to be employed.

In [51], the authors developed a real-time SOHc estimation method using an FNN based on the historical distribution of measured data over one year of tests of 18650 form factor cells. The method proposed in this work used data extracted from 10 different drive cycle profiles. In total, 44 datasets were created, eleven for each of the following temperatures: 10 °C, 25 °C, 45 °C, and 60°C. The historical distributions were based on 3D point clouds of battery current, voltage, and temperature. The relation between these three varies according to factors such as battery SOC and age. The patterns of the point clouds change as the battery ages and capacity changes. A key feature extraction idea of the paper is that rather than grouping data points based on voxel segments of the axes (current, voltage, and temperature), a k-means algorithm was employed to find more optimal sub-region volumes. This reduced the amount of FNN pattern classification necessary to estimate the SOHc. The optimal number of sub-regions determined in this work was 80. A histogram of counts in each sub-region served as inputs to the FNN. The FNN structure was composed of 80 inputs, a hidden layer of 80 neurons,

TABLE 2. Comparison of SOC estimation methods.

ML Method	Lowest Error (only at 25°C)	Data Profiles	Inputs(ψ) / Output (o)	Dataset Quality	Battery	Multi-Temperature
FNN[11]	0.33%(RMSE)@WLTC 0.27%(MAE) @WLTC	FTP75, NEDC, US06, GUDC, Highway, WLTC	ψ = $[V_{li(k)}, I_{li(k)}, T_{li(k)}, V'_{li(k)}, I'_{li(k)}, \sum I_{li(k)}, V_{la(k)}, I_{la(k)}, T_{la(k)}, V'_{la(k)}, I'_{la(k)}, \sum I_{la(k)}]$; o = $[SOC_{li(k)}; SOC_{la(k)}]$	***	LFP (12V, 8Ah)	No
FNN[13]	0.84%$^{++}$(MAE)@ US06 0.61% (MAE)@ HWFET	HWFET and US06	ψ = $[V_{(k)}, T_{(k)}, V_{avg(k)}, I_{avg(k)}]$; o = $[SOC_{(k)}]$	*****	[40]Li-ion Panasonic NCR18650PF	-20°C, -10°C, 0°C, 10°C, and 25°C
FNN w/ UKF[15]	1.4%(RMSE)@FUDS 2.5%(RMSE)@US06	FUDS, US06, DST	ψ = $[V_{(k)}, \ldots, V_{(k-4\tau)}, I_{(k)}, \ldots, I_{(k-4\tau)}, T_{(k)}, \ldots, T_{(k-4\tau)}]$; o = $[SOC_{(k)}]$	****	LFP (2.3Ah max)	0°C, 10°C, 20°C, 25°C, 40°C, and 50°C
FNN w/ECM[14]	0.33% (MAE)@FUDS	FUDS, DST	ψ = $[OCV_{(k)}]$; o = $[SOC_{(k)}]$	**	LFP (24V, 20Ah)	No
FNN w/ BSA[21]	0.81%(RMSE)@DST 0.91%(RMSE)@FUDS	FUDS, DST	ψ = $[V_{avg(k)}, I_{avg(k)}, T_{avg(k)}]$; o = $[SOC_{(k)}]$	***	NMC (3.6V, 2Ah)	0°C, 25°C, and 45°C
RBF w/ EKF[23]	~3% (RMSE)@CCC^{+}	Constant current charging (CCC)	ψ = $[V_{(k-1)}, I_{(k)}, SOC_{(k)}]$; o = $[V_{(k)}]$	*	Li-ion (1.2Ah)	No
RBF w/ H∞[25]	0.7%(RMSE) @CCC^{+}	Constant current charging (CCC)	ψ = $[V_{(k-1)}, I_{(k)}, SOC_{(k)}]$; o = $[V_{(k)}]$	*	Li-ion (1.2Ah)	No
RBF w/ UKF[26]	~3% (RMSE)@CCC^{+}	Constant current charging (CCC)	ψ = $[V_{(k-1)}, I_{(k)}, SOC_{(k)}]$; o = $[V_{(k)}]$	*	Li-ion (1.2Ah)	No
RBF w/ RSMO [27]	2.32%(RMSE)@UDDS^{+} 2.33%(RMSE)@HWY^{+}	UDDS, Highway	ψ = $[\hat{x}_1, \hat{x}_2, \hat{x}_3, \hat{x}_4]$; o = $[\hat{\psi}]$	**	Lithium-polymer, Turnigy (3.7V, 0.5Ah)	No
RBF w/ AEKF [29]	<2%(MAE)@DST^{+}	DST, HPPC	ψ = $[C^j{}_{rate}, SOC^j, \Delta Q^j]$ o = $[\delta^j]$	*	Lithium-polymer (3.7V, 32Ah)	No
RNN [38]	0.57%(MAE)@$^{++++}$	HWFET, UDDS, LA92, and US06	ψ = $[V_{(k)}, I_{(k)}, T_{(k)}]$; o = $[SOC_{(k)}]$	****	[40] Li-ion Panasonic NCR18650PF (3.6V, 2.9Ah)	0°C, 10°C, and 25°C
RNN [42]	0.32%(MAE)@LA92 0.86%(MAE)@ BJDST	Panasonic: HWFET, UDDS, LA92, and US06 Samsung: FUDS, US06, BJDST	ψ = $[V_{(k)}, I_{(k)}, T_{(k)}]$; o = $[SOC_{(k)}]$	*****	[40] Li-ion Panasonic NCR18650PF Li-ion Samsung 18650-20R	0°C, 10°C, 25°C, and 40 °C (Panasonic) 0°C, 25°C, and 45°C (Samsung)
RNN [46]	NMC: 0.77%(MAE)@$^{+}$ LFP: 1.72%(MAE)@$^{+}$	DST	ψ = $[V_{(k)}, I_{(k)}, T_{(k)}]$; o = $[SOC_{(k)}]$	**	BAK B18650CD A123 18650 (LFP)	0°C, 25°C, 20°C, 30°C, 40°C, 50°C
RNN[50]	LFP :0.53%(RMSE) @$^{++}$ LTO :0.70%(RMSE) @$^{++}$	Dynamic char./discharge profile^{++}	ψ = $[V_{(k)}, I_{(k)}]$; o = $[SOC_{(k)}]$	**	LFP (3.6V) LTO(2.6V)	0°C, 10°C, 25°C, and 40°C
ELM w/ AUKF[31]	0.4%(RMSE)@$^{++}$	Constant pulse discharging current^{++}	ψ = $[V_{(k-1)}, I_{(k)}, SOC_{(k)}]$; o = $[V_{(k)}]$	**	Samsung 2.6Ah	No
SVM[33]	0.4%(RMSE)@DST	DST	ψ = $[V_{(k)}, I_{(k)}, T_{(k)}]$; o = $[SOC_{(k)}]$	*	LFP (3.6V, 60Ah)	No

$^{+}$assumed as "room temperature" in the paper
$^{++}$ data acquired using a non-automotive dynamic charging/discharging profile
$^{+++}$ in the original paper, a typo shows the error as 0.084%.
$^{++++}$at 10°C

and a single output (SOHc). Fig. 13 shows an overview of the proposed approach. The FNN method was compared to two different SVM approaches. The first SVM used the same 3D inputs as the FNN, the other a combination of two 2D signals, e.g. current-temperature and voltage-temperature. The FNN was shown to have superior results. Practical challenges for the use of this method include lack of adaptability to adjust to cell-to-cell variations within a pack and the need to record and update the point cloud histogram distributions over the life of the battery pack.

A so-called structured neural network (SNN) was developed in [52] to compute SOH by estimation of internal parameters of a battery equivalent circuit model. The SNN is a variant of an FNN whose structure is guided by any existing battery model structure and knowledge. Compared to internal NN neurons, ECM parameters have a closer relation to the

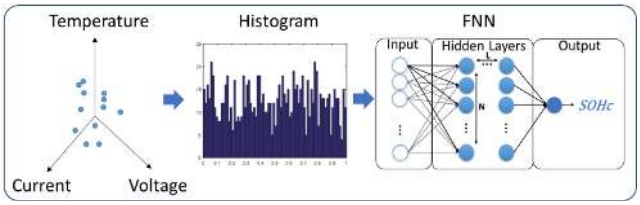

FIGURE 13. Point cloud distribution based SOH FNN [51].

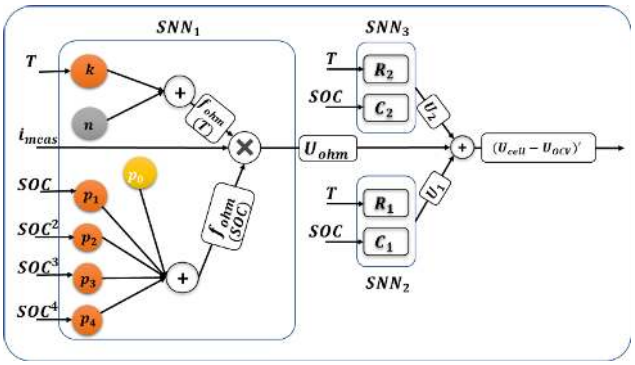

FIGURE 14. SNN schematic for internal resistance determination [52].

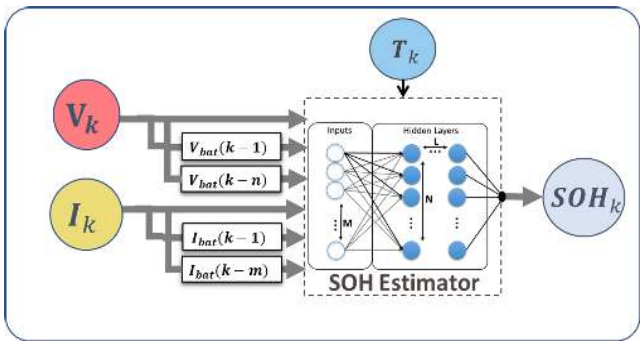

FIGURE 15. SOH estimator using ITDNN [53].

physical characteristics of the battery; for instance, the battery internal resistance variation over time can be correlated to the battery SOHr. Feature inputs to the SNN included SOC and its quadratic, cubic, and quartic powers. This enabled the usage of fourth-order polynomials in the SNN structure design. The overall SNN schematic is depicted in Fig. 14. In principle, training an SNN is expected to be easier since the global minimum is expected to be easier to find by choosing initial NN weight seed values based on model parameters rather than purely random values.

The data used to train the SNN was collected directly from a vehicle, a Mercedes Benz S400 Hybrid. The data collection started from a new vehicle, 0km, at the BOL up to 174000km at the EOL. Each dataset recorded had a length of about 5 hours, and a total of 33 datasets were collected. Part of the data, 70%, was used to train the SNN, and the rest was used to validate the model. EIS was used to validate the internal resistance estimated by the SNN. The work compared an

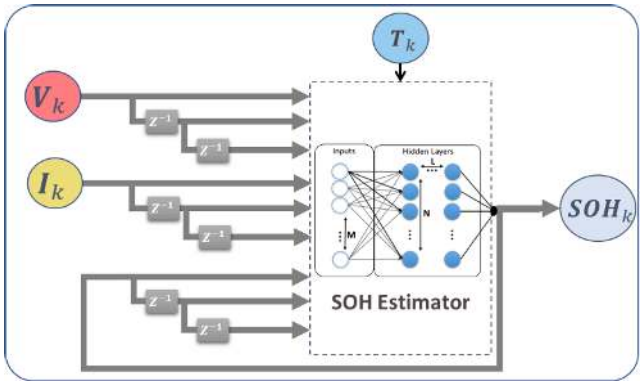

FIGURE 16. SOH estimator using DDRN [50], where the terminal voltage V_k, load current I_k and ambient temperature T_k are the inputs obtained by sensors, the delayed inputs were V_{k-1}, V_{k-2}, I_{k-1}, I_{k-2}, and recurrent inputs SOH_{k-1}, and SOH_{k-2}.

SNN with an Extended Kalman Filter approach that showed similar results. However, the SNN presented advantages in terms of computational speed and memory usage.

In [53], the authors used an FNN with time-delayed input data to estimate SOHc. It was referred to as an input time-delayed neural network (ITDNN). The usage of time-delayed inputs allows the NN better to model the dynamics and memory effects of a battery. The data used to estimate SOHc were based on the battery terminal voltage, current, time-delayed signals, and ambient temperature. An optimal time-delay of 20 seconds was determined for the voltage and current signals and shows the SOHc estimator structure. Fig. 15 shows the SOHc estimator structure where the FNN used was composed of 4 layers: 1 input layer, two hidden layers (L = 2), and one output layer. The hidden layers were formed of three and two neurons ($N_1 = 3$ and $N_2 = 2$), respectively, with each layer including a sigmoid activation function.

The dataset used to train and validate the model was divided into five milestones measured in hours: 0 hours (BOL), SOHc = 100%), 352 hours, 544 hours, 650 hours, and 650 hours (EOL, SOHc = 10%). Each dataset was generated at three separate ambient temperatures: 10°C, 25°C, and 40°C with currents of 6 A, 10 A, and 20 A. The battery used in this work was an LFP 20 Ah cell. A backpropagation algorithm was used to train the ITDNN.

The work presented in [54] used a similar approach of FNN with input time-delays employing a single hidden layer with ten neurons. Moreover, multiple time-delayed input signals were considered, and practical considerations such as the effect of capacity estimation error on SOC estimation was studied.

The authors in [55] have established that the geometric variation of the battery terminal voltage can be correlated to the battery SOHr. They showed that the terminal voltage slope of a battery reduces as its SOH decreases and its internal resistance increases. Therefore, a differential geometry-based approach using samples of the battery terminal voltage and its velocity, defined here as the voltage slope variation over time,

were used as inputs to train and validate a neural network capable of correlating these inputs to the battery SOHr. Data sets, containing data from cells at different ageing states, were used to train the neural network model. Another dataset from an LFP was used to validate the approach for other cell types. Results showed that the method was capable of estimating the battery SOH with accuracy around 1% Mean Absolute Error.

B. RECURRENT NEURAL NETWORK

SOH estimation involves tracking a slow battery ageing process from battery signals that exhibit dynamic states and memory. As a result, employing a recurrent neural network that contains internal memory is a natural approach to tackle SOH estimation.

A simple approach was presented in [50], where the authors built a dynamically driven recurrent network to estimate both the SOC and SOH of two Li-ion batteries. The RNN SOC estimation portion was described in the previous section. The SOHc estimate is fed back as delayed recurrent inputs; this gives the DDRN an associative memory feature, which is responsible for reducing the amount of data necessary to encode the dynamics in the network parameters. Other inputs to the RNN, include voltage, current, temperature, and time-delayed voltage and current. Fig. 16 shows the DDRN structure for SOH estimation.

The battery life in this work was measured for several cycles versus terminal voltage. Each cycle was acquired after placing the battery in a climate chamber at 60°C for a week to accelerate ageing, and then the batteries were charged and discharged at 25°C ambient temperature with the terminal voltage being measured and recorded every second during the discharge.

The training dataset consisted of four milestones: 100 cycles, 200 cycles, 1600 cycles, and 1800 cycles, where the 100 cycles milestone was deemed battery beginning of life and 1800 cycles as the end of life. The validation dataset employed seven milestones, and it was divided as follows 300, 500, 700, 800, 1000, 1200, and 1400 cycles. The structure of the DDRN was composed of an input, a single hidden layer (L = 1) and a single output. The hidden layer had 15 neurons (N = 15) with a sigmoid function as its activation function. The authors developed their discharge and charge power profiles for this work but they may not be a good representation of the xEV application domain. Therefore, the effectiveness of this approach needs to be further investigated. As the SOC and SOH estimators were independently trained using the same input vector but with different objective functions, no integration between SOC and SOH estimations were explored. With a larger and more dynamic dataset, there may be some benefits to integrating SOC and SOH estimation and this is recommended as an area of future work.

In [56], the authors created a novel approach to estimate the SOH based on a series of sequential snapshots of the battery current and voltage over time. This new approach aims to surpass the problems of the historical distribution discussed in the authors' previous work using an FNN approach [51]. The snapshot-based method takes into consideration the values of the battery current and terminal voltage within a window segment, with a fixed horizon width that shifts along with time. Moreover, this sliding window calculation happens only during charging, as it is considered to be a more stable and predictable condition than discharging. The proposed method utilizes LSTM layers similar to those shown in Fig. 7. The output of this LSTM block, shown in Fig. 17 is a set of vectors whose elements correspond to rolling time windows at different points in time, e.g. the first corresponds to the first window segment, and the last is shifted to reach up to the most recent point in time. A pooling block processes the output vectors of the LSTM blocks. Three different approaches for this block are possible; the first directly passes the most recent vector, the second averages all input vectors, the third is a bidirectional approach that performs an averaging of a kind of forward/reverse elementwise multiplication. This latter method aims to mitigate an often mentioned vanishing problem [36]. Finally, the pooling layer output is fed into a linear regression layer to estimate the SOHc.

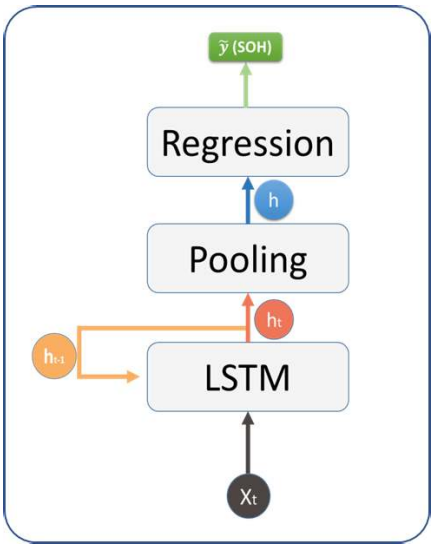

FIGURE 17. SOHc estimation architecture based on snapshot approach employing LSTM and linear regression [55].

The neural network structure was trained using backpropagation to update the weights and bias in each layer, aiming to minimize the error between a SOHc reference value and the estimated SOHc. Two other variations of this method were presented, including a merge with the historical distribution method (FNN approach) and the use of a BiLSTM. A dataset of 40 dynamic drive profiles tested at four different ambient temperatures (10, 25, 45, and 60°C) was employed. The batteries were aged via cycling until 70% of their original capacity remaining. The proposed framework was empirically verified, obtaining average error not higher than 0.0765 Ah on the testing dataset investigated at all temperatures.

In [57], the authors have also used an LSTM to estimate the battery SOHc where it was trained using a 2.3Ah LFP

TABLE 3. Publicly available battery datasets.

Dataset Repository	Reference
Li-ion Panasonic NCR18650PF	[40]
Li-ion -NASA Ames Prognostics Data Repository	[58]
Li-ion LFP A123 (APR18650M1A)	[72]
Li-ion LG 18650HG2	[73]

cell dataset, simulated from an electrochemical model of the cell at different SOH's. The data used to train the LSTM was based on the correlation of the cell capacity variation, voltage, current, and temperature. The dataset used to train the model was obtained by simulating an ageing procedure using the LFP electrochemical model, which includes submitting the model to high currents and temperature inputs. Then the SOHc was estimated only during charging profiles from the model simulated dataset. As ML can only be as good as the data used to train it, the dataset generated from a model should have a certain amount of error added to it, ensuring the estimation method has data representative of a real application. As an alternative to model-generated data, publicly available datasets can be used as well, as listed in Table 3. For example, a dataset from several Li-ion cells, provided by NASA Prognostics Center of Excellence [58] can be downloaded and used as the author did in a similar work [59].

The authors in [60] have developed and validated a model based on an LSTM to estimate both SOC and battery internal resistance (SOHr) simultaneously, meaning that it has two outputs instead of only one. The internal resistance data was first obtained from an ECM model implemented for this purpose. The inputs to the LSTM based model are the current, temperature, voltage, and voltage variation, which is the voltage value calculated from its difference at time step t and $t-1$, or just $U_t = V_t - V_{t-1}$. The relevance of the voltage variation was tested and shown to be valuable to improve model accuracy. The authors did not mention much detail about the chemistry of the Li-ion cell used besides some of its characteristics, e.g., Nominal capacity 2Ah, 18650 formats, nominal voltage 3.6V. The dataset used to train and validate the approach was obtained from the Li-ion cell by cycling the battery with US06, DST, and FUDS profiles at 0°C, 25°C, and 45°C. Only US06 and DST data were used to train the model, and FUDS was used to test. Although the method was shown to perform better in comparison to other ML models, a constraint regarding this approach is related to the accuracy of the internal resistance obtained from the ECM, as the LSTM can only be as accurate as of its objective function. Therefore another method, such as EIS, could be used to validate or determine the accuracy of the values generated by the ECM.

The authors in [61] have used EIS to determine and validate the parameters of an ECM capable of finding correlations with the Li-ion SOC, then developed an RNN to predict

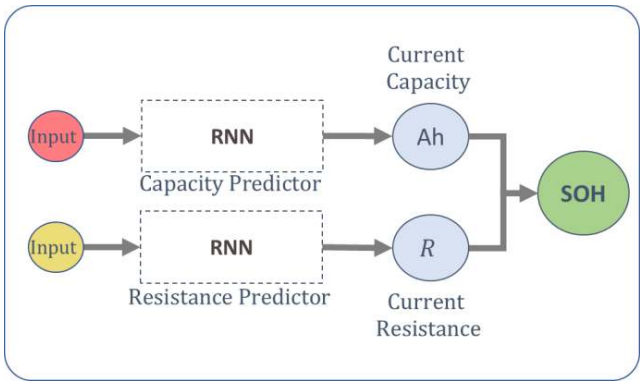

FIGURE 18. SOH estimation architecture based on battery capacity and resistance estimation using RNN [61].

the SOH of the Li-ion battery based on both the battery capacity fade and increase of its equivalent series resistance. The criteria of the battery EOL in this work is either when the capacity decreases 20% or when its equivalent resistance increases 100%, based on the battery BOL values. Datasets were experimentally obtained through months of tests by placing an NCA Li-ion cell under an accelerating ageing test protocol, which included a combination of ambient temperature varying from 40°C to 50°C, currents from 65A to 130A, and SOC from 20% to 40%. These datasets were finally used to train RNNs capable of estimating the battery capacity and equivalent resistance and combined to estimate SOH, as shown in Fig. 18. The RNNs were trained and tested by using cell temperature, current, SOC variation, and the capacity and resistance of previous time steps. The SOH estimator model has shown an accurate prediction of the battery SOH when compared to the experimental data, obtaining less than 1% mean squared error (MSE) on both capacity and resistance estimations.

C. RADIAL BASIS FUNCTIONS

A sparse bayesian predictive modelling (SBPM) algorithm can be used to identify the nonlinear relation of different features within a dataset. In [62], the authors used an SBPM to determine the relationship between the battery capacity and voltage sequence sample entropy, where the SBPM employs the concept of radial basis functions in its design. An HPPC procedure was used for testing a set of battery cells. The sample entropy assesses the dependency of a given data point on values of previous points and is averaged over the entire time-series [63]. In this case, the sample entropy is used to identify the pattern of the battery terminal voltage over time. The proposed SBPM-based method procedure is shown in Fig. 19.

The SBPM was trained and tested using data collected from NMC Li-ion cells (Panasonic UR14650P) at ambient temperatures of $10°C$, $22°C$, and $35°C$. The SBPM was also compared to an SVM, which like the SBPM, also adopted a radial basis function to correlate the nonlinear relationship between the capacity loss and the sample entropy. It was

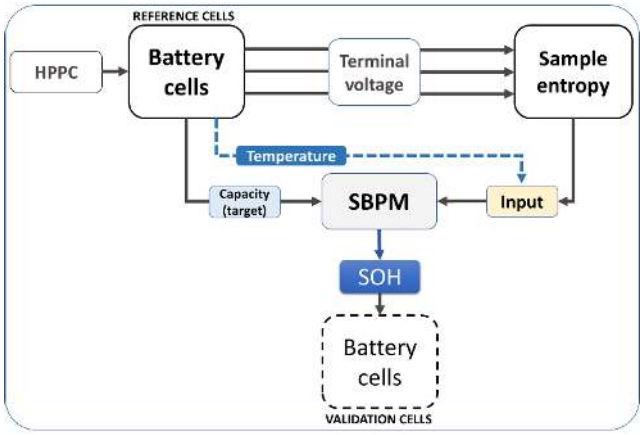

FIGURE 19. SBPM diagram to estimate the SOHc [62].

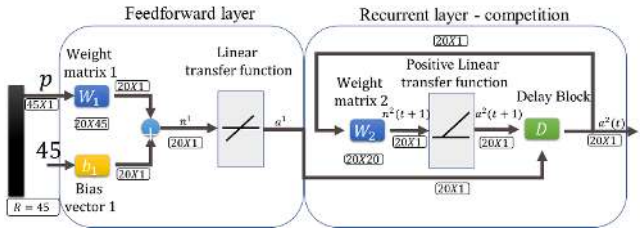

FIGURE 20. Hamming Neural Network [64].

observed that as the sample entropy increases, the capacity decreases.

D. HAMMING NEURAL NETWORK

A Hamming neural network (HNN) contains both an FNN and an RNN, and an example is shown in Fig. 20. The HNN has found extensive applications in pattern recognition, specifically binary pattern recognition. In [64], a Hamming Network was used in cooperation with a Dual Extended Kalman Filter (DEKF) to estimate SOC, capacity (SOHc) and resistance (SOHr). An equivalent circuit modelling approach was employed in the paper.

The HNN was used to estimate the ECM parameters based on charge/discharge voltage patterns, capacity patterns, and how they change over time. The parameters estimated were fed to a DEKF to perform battery state/parameter estimation. The HNN used reference patterns experimentally extracted from 20 Samsung 18650 Li-ion batteries tested at an ambient temperature of 27°C.

The battery data patterns were classified into 15 different categories. To be suitable for use in the HNN, the data needed to be transformed into binary arrays with elements of −1 or 1. The feedforward layer computes the internal product with the input pattern data, and the recurrent layer is responsible for outputting the dominant response using the winner-take-all principle [43]. After the HNN determines which of the predetermined patterns is the closest to an arbitrarily selected battery, the corresponding ECM parameters are selected, e.g. resistance $R^{selected}$. Resistance based SOHr was calculated as

$$SOH_r = \left| \frac{R^{selected} - R^{aged}}{R^{fresh} - R^{aged}} \right| \tag{6}$$

where $R^{selected}$ is the resistance of an arbitrarily selected battery determined by the HNN, R^{aged} is the resistance of an aged or EOL battery and R^{fresh} is the resistance of a new BOL battery.

Like many machine learning approaches, a significant part of the effort comes in the form of data acquisition and preparation before the data is ready to be used in the HNN. Moreover, the experimental results in this research were limited to a single temperature. Additional sophistication of the approach would be needed to handle an expanded temperature range and the resulting change in ECM parameters [65].

E. SUPPORT VECTOR MACHINE

The SVM was initially introduced in section II.D. for SOC estimation. This section will focus on methods using the SVM applied to xEV SOH estimation, including the work presented by the authors in [66], which uses an SVM to estimate SOHc and SOHr. For [66], data were acquired from the vehicle battery-based on charge and discharge profiles at four different temperatures (0°C, 10°C, 30°C, and 40°C). The data was used to train and validate the SOH estimation method based on both battery capacity and internal resistance variation. The SVM was initially trained to estimate the battery voltage drop response during 10s discharge pulses to calculate the battery resistance variation (SOHr) and capacity variation (SOHc) during C/3 partial or full discharge profiles. The inputs for the SVM were the battery current, temperature and SOC. The SOH estimation accuracy provided by the SVM was calculated from the measured values to be 0.63% RMSE for SOHc and 6.2% RMSE for SOHr. Computational performance measurements were also provided, showing potential viability for onboard vehicular applications.

Another work using an SVM to estimate SOH was presented in [67]. In this case, the authors combined an ECM with a relevance vector machine (RVM) and particle filter (PF) to estimate the SOC, SOH, and remaining-useful-life (RUL) of Li-ion batteries. The RVM, a supervised learning machine used in this case for regression, was trained to adaptively change the ECM internal parameters as the battery ages or fault processes occur. The data used to train the RVM was obtained from cycle-life tested 18650 Li-ion cells. EIS and various sensors were utilized to acquire the battery data, including but not limited to voltage, current, and temperature. Once trained, the RVM combined with the PF could generate a probability distribution over time to anticipate operational conditions and predict the SOH and RUL. Another work, presented in [68], proposed a new method combining the estimation of both SOC and SOH using an adaptive sigma point Kalman filter and an SVM. The work acknowledges the interdependence of SOC and SOH, which is likewise mentioned by many of the papers in this section. It is concluded

TABLE 4. Comparison of SOH methods.

ML Method	Lowest Error (only at 25°C)	SOH approach	Battery	Multi-Temperature consideration.
FNN w/ k-means[51]	SOHc: 0.66%(RMSE)	Based on capacity loss during charging	Li-ion 18650 3.1Ah	0°C, 10°C, 25°C, 45°C, and 60°C
RNN(LSTM)[56]	SOHc: 0.96%(RMSE) @ Validation R1 dataset	Based on capacity loss during charging	Li-ion 18650 3.1Ah	0°C, 10°C, 25°C, 45°C, and 60°C
DDRN[50]	SOHc: 0.1126Ah (RMSE) LFP@EOL SOHc: 0.34Ah (RMSE) LTO@EOL	Based capacity loss and number cycles	LFP (3.6V) LTO(2.6V)	25°C and 60°C (for accel. ageing)
FNN[55]	SOHr: 0.81% (MAE) LFP	Based on the internal resistance extracted from voltage variation	Li-ion IFP1865140	25°C
RNN[61]	SOHc: 0.46% (MSE) SOHr: 0.29%(MSE)	Based on Capacity and resistance estimation	NMC Li-ion (100Ah, Pouch))	40°C, and 50°C
SBPM[62]	SOHc: 1.38% (average relative capacity error)	Based capacity loss and sample entropy	NMC Li-ion Panasonic UR14650P (3.7V, 0.94Ah)	10°C, 22°C, and 35°C
FNN (SNN) w/ ECM[52]	0.32% (mean voltage deviation)@13,000km 0.28% % (mean voltage deviation)@80,000km	Based on ECM internal resistance estimation	Li-ion Saft VL6P (3.6V, 6.5 Ah)	23°C up to 50°C were considered
HNN w/ DEKF[64]	-	Based on ECM internal resistance estimation	Li-ion Samsung 18650(1.3 Ah)	No
SVM[66]	SOHc: 0.63%(RMSE) SOHr: 6.2% (RMSE)	Based on capacity and resistance variation	Li-ion Enerdel (17.5Ah, 2.5V, Pouch)	0°C to 40°C
DBN[70]	SOHr: <5%(MAE)	Based on resistance	Li-Mn (3.7V, 6Ah)	25°C and 55°C
BN[71]	SOHr: 0.28% (Avg Error) SOHr: 1.15% (Std Dev.)	Based on resistance	Li-Co (3.7V, 2.4Ah)	1°C and 23°C

that an accurate estimation of SOC or SOH can benefit the estimation of the other.

The authors in [69] have developed a model based on SVM, which is capable of learning and estimating SOHc online from battery voltage data acquired during charge, although only from a monotonic section of the data. The SVM strongly depends on finding the appropriate coefficient β; therefore, by adjusting the value of β as the battery ages, it is possible to adapt the SVM to update the SOHc properly. The initial value of β and the support vectors are determined using regression with the BOL battery data (voltage and battery capacity). During online operation, the coefficient β is updated using a least-squares algorithm. Segments of about 15 minutes in length are shown to be sufficient for the SVM to check for correlation within the data and to update the model parameters. This proposed approach is of interest because it avoids the need for online training, which is very computationally costly and hence avoided or merely impractical. The dataset was experimentally acquired from two NMC cells, where they were repeatedly cycled 60 times at 1C and 50°C and discharged at 25°C at 0.33C and 0.5C rates to measure capacity. This cycling sequence was repeated until the batteries reached 80% of their original capacity.

F. BAYESIAN NETWORK

A Bayesian network has the objective to find causation based on conditional dependencies by computing the probabilistic relationship between variables, and its dynamic version also considers the relationship at each sequential timestep. In [70], the authors have applied a Dynamic Bayesian Network (DBN) using only the observed battery terminal voltage to estimate the battery SOH. The DBN model was trained using data from Li-ion cells at different ageing states and constant current charging process with error not greater than 5%. Another similar work using a probabilistic distribution based on a Bayesian network (BN) was presented in [71]. The network uses the constant current time, voltage drop, and OCV after a CC/CV charge cycle and a rest period to estimate the SOH from the data extracted from 110 Li-ion batteries, where data from 100 were used to train and 10 to test the method. The accuracy obtained from the test was an average error of 0.28%.

G. COMPARISON OF SOH METHODS

Several characteristics of some of the techniques and research works presented in this section are summarized in Table 4, including the error for the SOHc, SOHr, or other SOH methods investigated, the battery type, and the temperatures considered. Almost all of the proposed methods are able to estimate capacity or resistance with 1% or less error, showing they are all promising candidates for SOH estimation. Two of the best methods are the FNN w/ k-means and RNN(LSTM) methods presented in [51] and in [56], which have low errors of 0.66% and 0.96% respectively despite the challenging multi-temperature dataset used to train and validate the networks.

It is challenging to draw more specific comparative conclusions about the methods, though, because of the differences between datasets, battery types, test conditions, and target criteria. As previously discussed in section II-F, ML models are data-driven algorithms and, therefore, the quality of the data used to train and validate is undoubtedly one of the essential aspects to be considered. Many of the works presented in this section have used datasets that are only good for preliminary studies, but insufficient to be used to compare methods intended to be applied to an xEV application. Therefore it is recommended that future ML SOH estimation works use publicly available datasets, as shown in Table 3, or share their datasets so others may benchmark their methods against the prior art. The dataset available in [72], for example, was obtained from 124 LFP cells acquired at fast-charging conditions at varying SOC ranges. The training guidelines suggested in section II-F can as well be applied to SOH estimation.

IV. CONCLUDING REMARKS

Based on the studies presented and summarized in this work, a wide range of machine learning approaches are suitable for the estimation of battery SOC and SOH. Many of the studies presented in this review did not use data with sufficient realistic dynamics that usually occur in a real xEV application. For example, only three studies, including the contribution of this work in section II-F, validated their method at negative ambient temperatures, where the estimation of SOC and SOH is even more challenging. Simplified comparisons were made among the different SOC and SOH estimation methods, providing some general insight with each work and showing that in general SOC and SOH can be estimated with an error of around 1%.

The studies reviewed also highlight the importance and challenge of collecting and preparing the data used to train and validate the algorithms; this is a crucial and challenging task when using data-driven algorithms. The data collection process can require months or years of testing, especially when SOH estimation is the objective. Despite the increasing amount of data being generated and the recent advances in the ML, their use and efficiency are still limited by not only the quantity but also the quality of the data. The computational complexity required to train and deploy ML-based models should be further investigated and compared in future work since it hasn't been addressed consistently within the surveyed work.

Many publications have used datasets that are good for preliminary studies but can be insufficient to compare methods intended for xEV application. Therefore, a table referencing publicly available datasets has been presented to facilitate the access to high-quality data and hence help improve further the quality of future works in the field. Additionally, the importance of the intrinsic random nature of the NN training process and the resultant variation of its accuracy was demonstrated by repeating the training of two different NNs fifty times. A simple set of guidelines is suggested to be followed when training and comparing ML algorithms, which considers the use of the same validation dataset, the number of ML fitted algorithm parameters and training process repetitions.

REFERENCES

[1] Z. Yang. (2017). *Improving the Conversions Between the Various Passenger Vehicle Fuel Economy/CO_2 Emission Standards Around the World*. International Council on Clean Transportation. Accessed: Jan. 1, 2017. [Online]. Available: https://www.theicct.org/blogs/staff/improving-conversions-between-passenger-vehicle-efficiency-standards

[2] B. Bilgin, P. Magne, P. Malysz, Y. Yang, V. Pantelic, M. Preindl, A. Korobkine, W. Jiang, M. Lawford, and A. Emadi, "Making the case for electrified transportation," *IEEE Trans. Transport. Electrific.*, vol. 1, no. 1, pp. 4–17, Jun. 2015.

[3] A. M. Andwari, A. Pesiridis, S. Rajoo, R. Martinez-Botas, and V. Esfahanian, "A review of battery electric vehicle technology and readiness levels," *Renew. Sustain. Energy Rev.*, vol. 78, pp. 414–430, Oct. 2017.

[4] M. A. Hannan, M. S. H. Lipu, A. Hussain, and A. Mohamed, "A review of lithium-ion battery state of charge estimation and management system in electric vehicle applications: Challenges and recommendations," *Renew. Sustain. Energy Rev.*, vol. 78, pp. 834–854, Oct. 2017.

[5] A. Emadi, *Advanced Electric Drive Vehicles*. New York, NY, USA: CRC Press, 2015.

[6] R. Zhang, B. Xia, B. Li, L. Cao, Y. Lai, W. Zheng, H. Wang, and W. Wang, "State of the art of lithium-ion battery SOC estimation for electrical vehicles," *Energies*, vol. 11, no. 7, p. 1820, 2018.

[7] M. Berecibar, I. Gandiaga, I. Villarreal, N. Omar, J. Van Mierlo, and P. Van den Bossche, "Critical review of state of health estimation methods of li-ion batteries for real applications," *Renew. Sustain. Energy Rev.*, vol. 56, pp. 572–587, Apr. 2016.

[8] S. Zuboff, *The Age of Surveillance Capitalism: The Fight for a Human Future at the New Frontier of Power*, 1st ed. New York, NY, USA: PublicAffairs, 2019.

[9] I. Goodfellow, Y. Bengio, and A. Courville, *Deep Learning*. Cambridge, MA, USA: MIT Press, 2016.

[10] A. Shrestha and A. Mahmood, "Review of deep learning algorithms and architectures," *IEEE Access*, vol. 7, pp. 53040–53065, 2019.

[11] C. Vidal, M. Haußmann, D. Barroso, P. M. Shamsabadi, A. Biswas, E. Chemali, R. Ahmed, and A. Emadi, "Hybrid energy storage system state-of-charge estimation using artificial neural network for micro-hybrid applications," in *Proc. IEEE Transp. Electrific. Conf. Expo (ITEC)*, Long Beach, CA, USA, Jun. 2018, pp. 1075–1081.

[12] H. Liu, A. Gegov, and M. Cocea, *Rule Based Systems for Big Data*, vol. 13. Cham, Switzerland: Springer, 2016.

[13] E. Chemali, P. J. Kollmeyer, M. Preindl, and A. Emadi, "State-of-charge estimation of li-ion batteries using deep neural networks: A machine learning approach," *J. Power Sour.*, vol. 400, pp. 242–255, Oct. 2018.

[14] X. Dang, L. Yan, H. Jiang, X. Wu, and H. Sun, "Open-circuit voltage-based state of charge estimation of lithium-ion power battery by combining controlled auto-regressive and moving average modeling with feedforward-feedback compensation method," *Int. J. Electr. Power Energy Syst.*, vol. 90, pp. 27–36, Sep. 2017.

[15] W. He, N. Williard, C. Chen, and M. Pecht, "State of charge estimation for li-ion batteries using neural network modeling and unscented Kalman filter-based error cancellation," *Int. J. Electr. Power Energy Syst.*, vol. 62, pp. 783–791, Nov. 2014.

[16] C. Vidal, O. Gross, R. Gu, P. Kollmeyer, and A. Emadi, "xEV Li-ion battery low-temperature effects—Review," *IEEE Trans. Veh. Technol.*, vol. 68, no. 5, pp. 4560–4572, May 2019.

[17] C. Chen, R. Xiong, R. Yang, W. Shen, and F. Sun, "State-of-charge estimation of lithium-ion battery using an improved neural network model and extended Kalman filter," *J. Cleaner Prod.*, vol. 234, no. 5, pp. 1153–1164, Oct. 2019.

[18] J. Yang, C. Du, T. Wang, Y. Gao, X. Cheng, P. Zuo, Y. Ma, J. Wang, G. Yin, J. Xie, and B. Lei, "Rapid prediction of the open-circuit-voltage of lithium ion batteries based on an effective voltage relaxation model," *Energies*, vol. 11, no. 12, p. 3444, 2018.

[19] Y. Hu and Z. Wang, "Study on SOC estimation of lithium battery based on improved BP neural network," in *Proc. 8th Int. Symp. Next Gener. Electron. (ISNE)*, Oct. 2019, pp. 1–3.

[20] J. Remmlinger, M. Buchholz, M. Meiler, P. Bernreuter, and K. Dietmayer, "State-of-health monitoring of lithium-ion batteries in electric vehicles by on-board internal resistance estimation," *J. Power Sour.*, vol. 196, no. 12, pp. 5357–5363, Jun. 2011.

[21] M. A. Hannan, M. S. H. Lipu, A. Hussain, M. H. Saad, and A. Ayob, "Neural network approach for estimating state of charge of lithium-ion battery using backtracking search algorithm," *IEEE Access*, vol. 6, pp. 10069–10079, 2018.

[22] S. Tong, J. H. Lacap, and J. W. Park, "Battery state of charge estimation using a load-classifying neural network," *J. Energy Storage*, vol. 7, pp. 236–243, Aug. 2016.

[23] M. Charkhgard and M. Farrokhi, "State-of-charge estimation for lithium-ion batteries using neural networks and EKF," *IEEE Trans. Ind. Electron.*, vol. 57, no. 12, pp. 4178–4187, Dec. 2010.

[24] M. Shahriari and M. Farrokhi, "Online state-of-health estimation of VRLA batteries using state of charge," *IEEE Trans. Ind. Electron.*, vol. 60, no. 1, pp. 191–202, Jan. 2012.

[25] A. Alfi, M. H. Zarif, and M. Charkhgard, "Hybrid state of charge estimation for lithium-ion batteries: Design and implementation," *IET Power Electron.*, vol. 7, no. 11, pp. 2758–2764, Nov. 2014.

[26] H. Gholizade-Narm and M. Charkhgard, "Lithium-ion battery state of charge estimation based on square-root unscented Kalman filter," *IET Power Electron.*, vol. 6, no. 9, pp. 1833–1841, Nov. 2013.

[27] X. Chen, W. Shen, M. Dai, Z. Cao, J. Jin, and A. Kapoor, "Robust adaptive sliding-mode observer using RBF neural network for lithium-ion battery state of charge estimation in electric vehicles," *IEEE Trans. Veh. Technol.*, vol. 65, no. 4, pp. 1936–1947, Apr. 2016.

[28] X. Chen, W. Shen, Z. Cao, and A. Kapoor, "Adaptive gain sliding mode observer for state of charge estimation based on combined battery equivalent circuit model," *Comput. Chem. Eng.*, vol. 64, pp. 114–123, May 2014.

[29] F. Sun, R. Xiong, and H. He, "A systematic state-of-charge estimation framework for multi-cell battery pack in electric vehicles using bias correction technique," *Appl. Energy*, vol. 162, pp. 1399–1409, Jan. 2016.

[30] G.-B. Huang, Q.-Y. Zhu, and C.-K. Siew, "Extreme learning machine: Theory and applications," *Neurocomputing*, vol. 70, nos. 1–3, pp. 489–501, Dec. 2006.

[31] J. Du, Z. Liu, and Y. Wang, "State of charge estimation for li-ion battery based on model from extreme learning machine," *Control Eng. Pract.*, vol. 26, no. 1, pp. 11–19, May 2014.

[32] M. S. Hossain Lipu, M. A. Hannan, A. Hussain, M. H. Saad, A. Ayob, and M. N. Uddin, "Extreme learning machine model for state-of-charge estimation of lithium-ion battery using gravitational search algorithm," *IEEE Trans. Ind. Appl.*, vol. 55, no. 4, pp. 4225–4234, Jul. 2019.

[33] J. C. A. Anton, P. J. G. Nieto, C. B. Viejo, and J. A. V. Vilan, "Support vector machines used to estimate the battery state of charge," *IEEE Trans. Power Electron.*, vol. 28, no. 12, pp. 5919–5926, Dec. 2013.

[34] J. C. Álvarez Antón, P. J. García Nieto, F. J. de Cos Juez, F. Sánchez Lasheras, M. González Vega, and M. N. Roqueñí Gutiérrez, "Battery state-of-charge estimator using the SVM technique," *Appl. Math. Model.*, vol. 37, no. 9, pp. 6244–6253, May 2013.

[35] R. Pascanu, T. Mikolov, and Y. Bengio, "On the difficulty of training Recurrent Neural Networks," in *Proc. Int. Conf. Mach. Learn.*, Atlanta, GA, USA, 2013, pp. 1310–1318.

[36] S. Hochreiter and J. Schmidhuber, "Long short-term memory," *Neural Comput.*, vol. 9, no. 8, pp. 1735–1780, 1997.

[37] C. Olah. (2015). *Understanding LSTM Networks [Blog]*. Accessed: Jan. 27, 2020. [Online]. Available: https://colah.github.io/posts/2015-08-Understanding-LSTMs/

[38] E. Chemali, P. J. Kollmeyer, M. Preindl, R. Ahmed, and A. Emadi, "Long short-term memory networks for accurate state-of-charge estimation of li-ion batteries," *IEEE Trans. Ind. Electron.*, vol. 65, no. 8, pp. 6730–6739, Aug. 2018.

[39] A. Graves, A.-R. Mohamed, and G. Hinton, "Speech recognition with deep recurrent neural networks," in *Proc. IEEE Int. Conf. Acoust., Speech Signal Process.*, Vancouver, BC, Canada, May 2013, pp. 6645–6649.

[40] *Panasonic 18650PF Li-Ion Battery Data*. Accessed: Jan. 20, 2020. [Online]. Available: http://dx.doi.org/10.17632/wykht8y7tg.1#folder-96f196a8-a04d-4e6a-827d-0dc4d61ca97b

[41] C. Bian, H. He, and S. Yang, "Stacked bidirectional long short-term memory networks for state-of-charge estimation of lithium-ion batteries," *Energy*, vol. 191, Jan. 2020, Art. no. 116538.

[42] C. Li, F. Xiao, and Y. Fan, "An approach to state of charge estimation of lithium-ion batteries based on recurrent neural networks with gated recurrent unit," *Energies*, vol. 12, no. 9, p. 1592, 2019.

[43] F. Yang, X. Song, F. Xu, and K.-L. Tsui, "State-of-charge estimation of lithium-ion batteries via long short-term memory network," *IEEE Access*, vol. 7, pp. 53792–53799, 2019.

[44] A. Bonfitto, S. Feraco, A. Tonoli, N. Amati, and F. Monti, "Estimation accuracy and computational cost analysis of artificial neural networks for state of charge estimation in lithium batteries," *Batteries*, vol. 5, no. 2, p. 47, Jun. 2019.

[45] M. S. H. Lipu, M. A. Hannan, A. Hussain, M. H. M. Saad, A. Ayob, and F. Blaabjerg, "State of charge estimation for lithium-ion battery using recurrent NARX neural network model based lighting search algorithm," *IEEE Access*, vol. 6, pp. 28150–28161, 2018.

[46] F. Yang, W. Li, C. Li, and Q. Miao, "State-of-charge estimation of lithium-ion batteries based on gated recurrent neural network," *Energy*, vol. 175, pp. 66–75, May 2019.

[47] A. C. Caliwag and W. Lim, "Hybrid VARMA and LSTM method for lithium-ion battery state-of-charge and output voltage forecasting in electric motorcycle applications," *IEEE Access*, vol. 7, pp. 59680–59689, 2019.

[48] C. Vidal, P. Kollmeyer, E. Chemali, and A. Emadi, "Li-ion battery state of charge estimation using long short-term memory recurrent neural network with transfer learning," in *Proc. IEEE Transp. Electrific. Conf. Expo (ITEC)*, Novi, MI, USA, Jun. 2019, pp. 1–6.

[49] A. Khalid, A. Sundararajan, I. Acharya, and A. I. Sarwat, "Prediction of li-ion battery state of charge using multilayer perceptron and long short-term memory models," in *Proc. IEEE Transp. Electrific. Conf. Expo (ITEC)*, Novi, MI, USA, Jun. 2019, pp. 1–6.

[50] H. Chaoui and C. C. Ibe-Ekeocha, "State of charge and state of health estimation for lithium batteries using recurrent neural networks," *IEEE Trans. Veh. Technol.*, vol. 66, no. 10, pp. 8773–8783, Oct. 2017.

[51] G.-W. You, S. Park, and D. Oh, "Real-time state-of-health estimation for electric vehicle batteries: A data-driven approach," *Appl. Energy*, vol. 176, pp. 92–103, Aug. 2016.

[52] D. Andre, A. Nuhic, T. Soczka-Guth, and D. U. Sauer, "Comparative study of a structured neural network and an extended Kalman filter for state of health determination of lithium-ion batteries in hybrid electricvehicles," *Eng. Appl. Artif. Intell.*, vol. 26, no. 3, pp. 951–961, Mar. 2013.

[53] H. Chaoui, C. C. Ibe-Ekeocha, and H. Gualous, "Aging prediction and state of charge estimation of a $LiFePO_4$ battery using input time-delayed neural networks," *Electr. Power Syst. Res.*, vol. 146, pp. 189–197, May 2017.

[54] A. A. Hussein, "Capacity fade estimation in electric vehicle li-ion batteries using artificial neural networks," *IEEE Trans. Ind. Appl.*, vol. 51, no. 3, pp. 2321–2330, May 2015.

[55] J. Wu, Y. Wang, X. Zhang, and Z. Chen, "A novel state of health estimation method of li-ion battery using group method of data handling," *J. Power Sour.*, vol. 327, pp. 457–464, Sep. 2016.

[56] G.-W. You, S. Park, and D. Oh, "Diagnosis of electric vehicle batteries using recurrent neural networks," *IEEE Trans. Ind. Electron.*, vol. 64, no. 6, pp. 4885–4893, Jun. 2017.

[57] A. Veeraraghavan, V. Adithya, A. Bhave, and S. Akella, "Battery aging estimation with deep learning," in *Proc. IEEE Transp. Electrific. Conf. (ITEC-India)*, Pune, India, Dec. 2017, pp. 1–4.

[58] B. Saha and K. Goebel. (2007). Battery Data Set. NASA Ames Prognostics Data Repository. NASA Ames Research Center. Moffett Field, CA, USA. [Online]. Available: http://ti.arc.nasa.gov/project/prognostic-data-repository

[59] Y. Choi, S. Ryu, K. Park, and H. Kim, "Machine learning-based lithium-ion battery capacity estimation exploiting multi-channel charging profiles," *IEEE Access*, vol. 7, pp. 75143–75152, 2019.

[60] C. Zhang, Y. Zhu, G. Dong, and J. Wei, "Data-driven lithium-ion battery states estimation using neural networks and particle filtering," *Int. J. Energy Res.*, vol. 43, no. 14, Aug. 2019, pp. 8230–8241, Paper er.4820.

[61] A. Eddahech, O. Briat, N. Bertrand, J.-Y. Delétage, and J.-M. Vinassa, "Behavior and state-of-health monitoring of li-ion batteries using impedance spectroscopy and recurrent neural networks," *Int. J. Electr. Power Energy Syst.*, vol. 42, no. 1, pp. 487–494, Nov. 2012.

[62] X. Hu, J. Jiang, D. Cao, and B. Egardt, "Battery health prognosis for electric vehicles using sample entropy and sparse Bayesian predictive modeling," *IEEE Trans. Ind. Electron.*, vol. 63, no. 4, pp. 2645–2656, Apr. 2016.

[63] J. S. Richman, D. E. Lake, and J. R. Moorman, "Sample entropy," *Methods Enzymol.*, vol. 384, pp. 172–184, Jan. 2004.

[64] J. Kim, S. Lee, and B. H. Cho, "Complementary cooperation algorithm based on DEKF combined with pattern recognition for SOC/capacity estimation and SOH prediction," *IEEE Trans. Power Electron.*, vol. 27, no. 1, pp. 436–451, Jan. 2012.

[65] P. Malysz, J. Ye, R. Gu, H. Yang, and A. Emadi, "Battery state-of-power peak current calculation and verification using an asymmetric parameter equivalent circuit model," *IEEE Trans. Veh. Technol.*, vol. 65, no. 6, pp. 4512–4522, Jun. 2016.
[66] V. Klass, M. Behm, and G. Lindbergh, "A support vector machine-based state-of-health estimation method for lithium-ion batteries under electric vehicle operation," *J. Power Sour.*, vol. 270, pp. 262–272, Dec. 2014.
[67] B. Saha, S. Poll, K. Goebel, and J. Christophersen, "An integrated approach to battery health monitoring using Bayesian regression and state estimation," in *Proc. IEEE Autotestcon*, Baltimore, MD, USA, Sep. 2007, pp. 646–653.
[68] P.-H. Michel and V. Heiries, "An adaptive sigma point Kalman filter hybridized by support vector machine algorithm for battery SoC and SoH estimation," in *Proc. IEEE 81st Veh. Technol. Conf. (VTC Spring)*, May 2015, pp. 1–7.
[69] X. Feng, C. Weng, X. He, X. Han, L. Lu, D. Ren, and M. Ouyang, "Online state-of-health estimation for li-ion battery using partial charging segment based on support vector machine," *IEEE Trans. Veh. Technol.*, vol. 68, no. 9, pp. 8583–8592, Sep. 2019.
[70] Z. He, M. Gao, G. Ma, Y. Liu, and S. Chen, "Online state-of-health estimation of lithium-ion batteries using dynamic Bayesian networks," *J. Power Sour.*, vol. 267, pp. 576–583, Dec. 2014.
[71] H.-T. Lin, T.-J. Liang, and S.-M. Chen, "Estimation of battery state of health using probabilistic neural network," *IEEE Trans Ind. Informat.*, vol. 9, no. 2, pp. 679–685, May 2013.
[72] K. A. Severson, P. M. Attia, N. Jin, N. Perkins, B. Jiang, Z. Yang, M. H. Chen, M. Aykol, P. K. Herring, D. Fraggedakis, M. Z. Bazant, S. J. Harris, W. C. Chueh, and R. D. Braatz, "Data-driven prediction of battery cycle life before capacity degradation," *Nature Energy*, vol. 4, no. 5, pp. 383–391, May 2019.
[73] P. Kollmeyer, C. Vidal, M. Naguib, and M. Skells, "LG 18650HG2 li-ion battery data and example deep neural network xEV SOC estimator script," 2020, Mendeley Data.

CARLOS VIDAL (Student Member, IEEE) received the B.S. degree in electrical engineering from the Federal University of Campina Grande (UFCG), in 2005, the M.B.A. degree, with concentration in project management, from Getulio Vargas Foundation (FGV), in 2007, and the M.A.Sc. degree in civil and environmental engineering from the Federal University of Pernambuco (UFPE), Brazil, in 2015. He is currently pursuing the Ph.D. degree in mechanical engineering with McMaster University, Hamilton, ON, Canada. In 2017, he joined the McMaster Institute for Automotive Research and Technology (MacAUTO), McMaster University. Before joining McMaster, he has been gathering industry experience from several engineering and management positions. His main research areas include artificial intelligence, modeling, and energy storage applied to electrified vehicles and batteries management systems.

PAWEL MALYSZ (Senior Member, IEEE) received the B.Eng. degree *(summa cum laude)* in engineering physics, and the M.A.Sc. and Ph.D. degrees in electrical engineering from McMaster University, Hamilton, ON, Canada, in 2005, 2007, and 2011, respectively. In 2015, he was appointed as an Adjunct Assistant Professor with the Department of Electrical and Computer Engineering, McMaster University. He was a part of the Mechanical Engineering Department, Lawrence Technological University, Southfield, MI, USA, as an Adjunct Professor, where he taught a course in hybrid electric and all-electric vehicles. He holds four patents and has published over 40 peer-reviewed journal/conference papers. His research interests include energy systems, battery management software design, electrified transportation, and advanced control engineering. Throughout his graduate studies, he received scholarship awards such as the Ontario Graduate Scholarship, Queen Elizabeth II Graduate Scholarship, and the National Science and Engineering Research Council (NSERC) of Canada graduate scholarships. From 2012 to 2014, he was a Principal Research Engineer at the McMaster Institute for Automotive Research and Technology, a Canada Excellence Research Centre. He is a licensed Professional Engineer (P.Eng.) in the province of Ontario, a Golden Key International Honor Society member, and currently a Senior Technical Specialist at Fiat Chrysler Automobiles (FCA) US LLC, Auburn Hills, MI, USA. He co-received the Chrysler Innovation Award, in 2014.

PHILLIP KOLLMEYER (Member, IEEE) received the B.S., M.S., and Ph.D. degrees in electrical engineering from the University of Wisconsin-Madison, Madison, WI, USA, in 2006, 2011, and 2015, respectively. As a graduate student, he built a prototype light-duty electric truck and led the development of a new energy storage test facility. He also performed a range of projects on hybrid energy storage, battery ageing, and battery and ultracapacitor modeling, and received two awards for his teaching in the electric machines and drives area. He is currently a Senior Principal Research Engineer with McMaster University, Hamilton, ON, Canada, where his focus is energy storage and electric drivetrain research for transportation applications.

ALI EMADI (Fellow, IEEE) received the B.S. and M.S. degrees (Hons.) in electrical engineering from the Sharif University of Technology, Tehran, Iran, in 1995 and 1997, respectively, and the Ph.D. degree in electrical engineering from Texas A&M University, College Station, TX, USA, in 2000. He is currently the Canada Excellence Research Chair Laureate with McMaster University, Hamilton, ON, Canada. He is also the Holder of the NSERC/FCA Industrial Research Chair in Electrified Powertrains and Tier I Canada Research Chair in Transportation Electrification and Smart Mobility. Before joining McMaster University, he was the Harris Perlstein Endowed Chair Professor of Engineering and the Director of the Electric Power and Power Electronics Center and Grainger Laboratories at Illinois Institute of Technology, Chicago, IL, USA, where he established research and teaching facilities as well as courses in power electronics, motor drives, and vehicular power systems. He was the Founder, Chairman, and President of Hybrid Electric Vehicle Technologies, Inc. (HEVT)—a university spin-off company of Illinois Tech. He is the principal author/coauthor of over 450 journal and conference papers as well as several books, including *Vehicular Electric Power Systems* (2003), *Energy Efficient Electric Motors* (2004), *Uninterruptible Power Supplies and Active Filters* (2004), *Modern Electric*, *Hybrid Electric*, and *Fuel Cell Vehicles* (2nd ed., 2009), and *Integrated Power Electronic Converters and Digital Control* (2009). He is also the Editor of the *Handbook of Automotive Power Electronics and Motor Drives* (2005) and *Advanced Electric Drive Vehicles* (2014). He has been a recipient of numerous awards and recognitions. He was the advisor for the Formula Hybrid Teams at Illinois Tech and McMaster University, which won the GM Best Engineered Hybrid System Award at the 2010, 2013, and 2015 competitions. He was the Inaugural General Chair of the 2012 IEEE Transportation Electrification Conference and Expo (ITEC) and has chaired several IEEE and SAE conferences in the areas of vehicle power and propulsion. He is the Co-Editor of the *Switched Reluctance Motor Drives* (2018). He is the founding Editor-in-Chief of the IEEE TRANSACTIONS ON TRANSPORTATION ELECTRIFICATION.